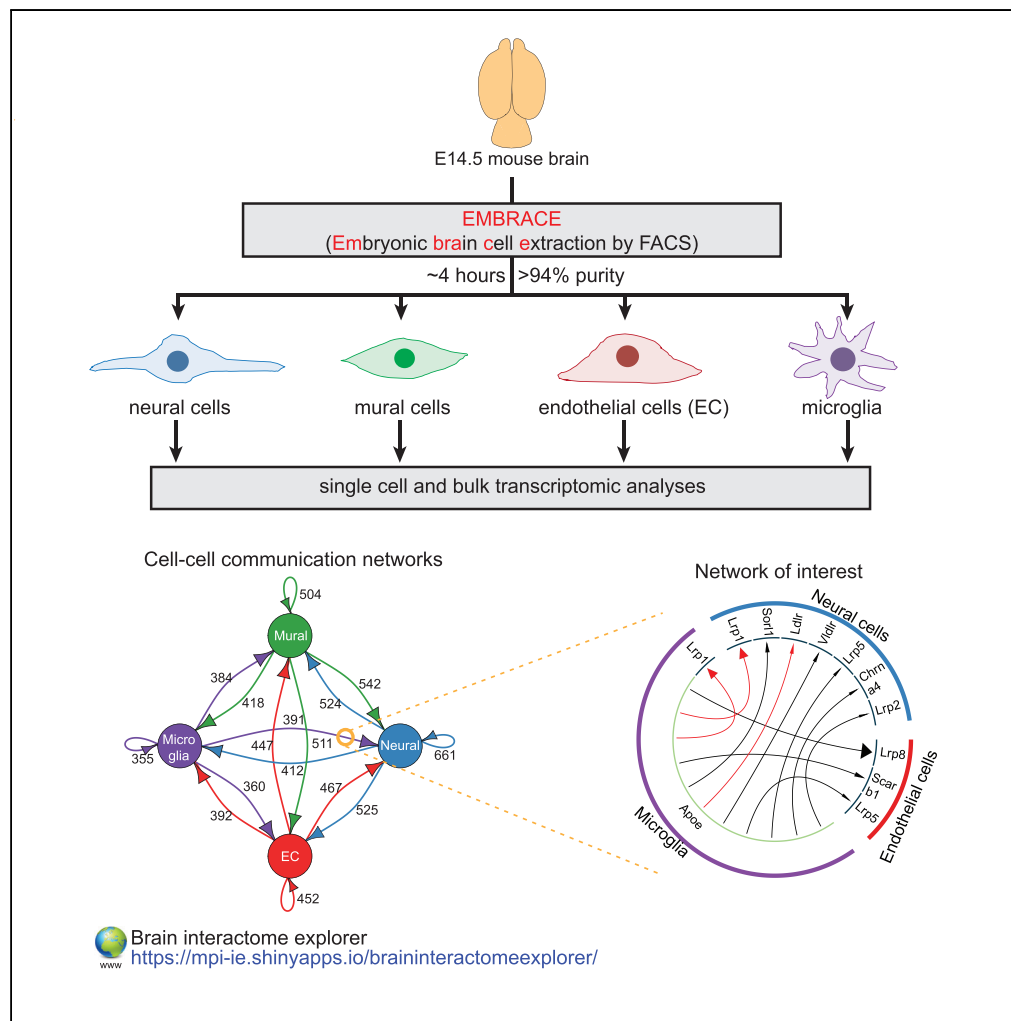


Article

Systematic Identification of Cell-Cell Communication Networks in the Developing Brain



Bilal N. Sheikh,
Olga Bondareva,
Sukanya
Guhathakurta, ...,
Dominic Grün,
Lutz Hein, Asifa
Akhtar

sheikh@ie-freiburg.mpg.de
(B.N.S.)
akhtar@ie-freiburg.mpg.de
(A.A.)

HIGHLIGHTS

Isolation of embryonic neural, mural, endothelial, and microglial cells to >94% purity

Transcriptome analyses of neural, vascular, and microglial cells from E14.5 brain

Generation of inter-cellular communication network with 1,710 unique interactions

Established "Brain interactome explorer," a searchable cell communication database

DATA AND CODE AVAILABILITY
GSE133079

Sheikh et al., iScience 21, 273–287
November 22, 2019 © 2019
The Author(s).
<https://doi.org/10.1016/j.isci.2019.10.026>



Article

Systematic Identification of Cell-Cell Communication Networks in the Developing Brain

Bilal N. Sheikh,^{1,4,*} Olga Bondareva,^{2,4} Sukanya Guhathakurta,^{1,3} Tsz Hong Tsang,^{1,3} Katarzyna Sikora,¹ Nadim Aizarani,^{1,3} Sagar,¹ Herbert Holz,¹ Dominic Grün,¹ Lutz Hein,² and Asifa Akhtar^{1,5,*}

SUMMARY

Since the generation of cell-type specific knockout models, the importance of inter-cellular communication between neural, vascular, and microglial cells during neural development has been increasingly appreciated. However, the extent of communication between these major cell populations remains to be systematically mapped. Here, we describe EMBRACE (embryonic brain cell extraction using FACS), a method to simultaneously isolate neural, mural, endothelial, and microglial cells to more than 94% purity in ~4 h. Utilizing EMBRACE we isolate, transcriptionally analyze, and build a cell-cell communication map of the developing mouse brain. We identify 1,710 unique ligand-receptor interactions between neural, endothelial, mural, and microglial cells *in silico* and experimentally confirm the APOE-LDLR, APOE-LRP1, VTN-KDR, and LAMA4-ITGB1 interactions in the E14.5 brain. We provide our data via the searchable "Brain interactome explorer", available at <https://mpi-ie.shinyapps.io/braininteractomeexplorer/>. Together, this study provides a comprehensive map that reveals the richness of communication within the developing brain.

INTRODUCTION

Embryonic development is a highly reproducible process that requires extensive communication between cells. Inter-cellular communication is particularly evident during the development and maturation of the mammalian brain. During embryonic development, human and murine brains consist primarily of neural stem cells that give rise to progenitors, which migrate into the developing cortex and differentiate into neurons (Jiang and Nardelli, 2016). In contrast, astrocytes and oligodendrocytes start to develop around the time of birth and are largely absent during prenatal development. In addition to the neural lineage, microglia, the resident immune cells of the central nervous system, as well as vascular endothelial cells and pericytes are also present in the developing brain (Alliot et al., 1999; Daneman et al., 2010b; Vasudevan et al., 2008). The presence and functionality of vascular cells and microglia is critical for proper neural development, and dysregulation of these cells results in severe neural disorders (Daneman et al., 2010b; Matcovitch-Natan et al., 2016; Mathys et al., 2017; Sengillo et al., 2013; Vasudevan et al., 2008). Indeed, neural cells not only communicate to impart particular cell fates upon each other (Barnabe-Heider et al., 2005; Yuzwa et al., 2016), but also communicate with developing vascular cells and microglia to guide their development (Haigh et al., 2003; Ma et al., 2017; Nikolakopoulou et al., 2013; Sellner et al., 2016). For instance, VEGF-A released by neural progenitor cells is detected by endothelial cells and is critical for proper angiogenesis and vascularization of the developing brain (Haigh et al., 2003). Similarly, endothelial cells are able to modulate the behavior of neural stem and progenitor cells (Crouch et al., 2015), as well as recruit vascular pericytes to ensure proper establishment of the blood-brain barrier (Hellstrom et al., 1999; Winkler et al., 2010). Simultaneously, pericytes provide differentiation signals for endothelial cells and modulate their function (Daneman et al., 2010b). Furthermore, microglia begin to enter the developing brain around E9 (Alliot et al., 1999; Stremmel et al., 2018) and modulate aspects of neural differentiation and synaptic structure (Nikolakopoulou et al., 2013; Paolicelli et al., 2011; Zhan et al., 2014). Despite the accumulation of evidence that interactions between neural cells, microglia, and vascular cells are critical for proper brain development, the identity of the molecules that mediate these inter-cellular interactions remains to be systematically mapped.

Fluorescence-activated cell sorting (FACS) is commonly used for the isolation and profiling of neural vascular cells and microglia. Microglia can be enriched using antibodies against CD11b and CD45 (Bennett et al., 2016; Datta et al., 2018; Mathys et al., 2017), whereas isolation of the mural cell population, which spans both pericytes and smooth muscle cells, typically relies on transgenic mice expressing fluorescent proteins under the *Pdgfrb* and *Cspg4* promoters (He et al., 2016; Vanlandewijck et al., 2018). Similarly,

¹Max Planck Institute of Immunobiology and Epigenetics, Stuebeweg 51, Freiburg 79108, Germany

²Institute of Experimental and Clinical Pharmacology and Toxicology, University of Freiburg, Albertstr. 25, Freiburg 79104, Germany

³Faculty of Biology, Albert Ludwig University of Freiburg, Freiburg 79104, Germany

⁴These authors contributed equally

⁵Lead Contact

*Correspondence:
sheikh@ie-freiburg.mpg.de
(B.N.S.),
akhtar@ie-freiburg.mpg.de
(A.A.)

<https://doi.org/10.1016/j.isci.2019.10.026>



studies have utilized transgenic approaches such as *Tie2-GFP* (Daneman et al., 2010a; Zhang et al., 2014) and *Cldn5-GFP* (Vanlandewijck et al., 2018) animals for the isolation of endothelial cells. Given the time-consuming nature of transgenic animal production and crossing to mouse models of interest, researchers have been attempting to establish antibody-based methods for the isolation of vascular cells. Antibodies against CD13 (Crouch and Doetsch, 2018) and PDGFR β (Epshtain et al., 2017) have recently been tested for the isolation of mural cells, whereas the use of antibodies against CD31 (PECAM1) is becoming more widespread for the isolation of endothelial cells (Crouch and Doetsch, 2018; Czupalla et al., 2018; Fan et al., 2014; Wang et al., 2019). The specificity of these markers has been confirmed using immunohistochemistry. However, the accuracy or purity of cell populations obtained from antibody-based FACS methods is yet to be quantifiably tested. Furthermore, given the importance of inter-cellular communication within the brain, a reliable and efficient method is still required to simultaneously isolate neural, vascular, and microglial cells to map changes in inter-cellular networks in genetically modified model systems.

In the current study, we describe EMBRACE (embryonic brain cell extraction using FACS), a method that allows for the simultaneous and rapid isolation of neural, mural, endothelial, and microglial cells from the embryonic brain. The combinations of cell-type specific markers utilized in EMBRACE permit it to achieve 94%–100% purity for each of the cell populations, which we validate through single cell RNA sequencing (scRNA-seq) analyses. To capture lowly expressed genes and to obtain better transcriptional resolution for in-depth analyses, we additionally perform low-input bulk RNA-seq on cell populations isolated by EMBRACE. Utilizing this transcriptomic data, we build a cell-cell communication network that reveals the richness and extent of communication within the developing brain.

RESULTS

Sorting Strategy for the Isolation of Neural, Microglial, and Vascular Cells

In the current study, we set out to establish a protocol for the simultaneous isolation of neural, mural, endothelial, and microglial cells and systematically map interactions between these four cell types. We chose to focus our efforts on the E14.5 mouse brain for these analyses. The neural population in the E14.5 embryo consists primarily of neural stem and progenitors cells as well as migrating neurons (Jiang and Nardelli, 2016). Thus, cell dissociation methods are unlikely to cause excessive cell death as is common with mature neuronal populations, which possess extensive neurites. Furthermore, microglial seeding of the brain begins around E9 and is completed by E14.5 (Stremmel et al., 2018), suggesting that microglia would already be present and likely interacting with their native neural environment in the E14.5 brain. Neural vascularization and angiogenesis are also evident at E14.5 with the presence of maturing endothelial cells, active migration of tip cells, as well as recruitment and differentiation of mural cells (Tata et al., 2015). In fact, blood-brain barrier (BBB) maturation is completed around E15.5, suggesting that analyses at E14.5 are likely to reveal key factors required for BBB maturation.

To identify the most efficient method to dissociate E14.5 embryonic brains into a single cell suspension, we tested a number of enzymatic and non-enzymatic methods. We identified the combination of Liberase and DNase I as the most reliable method that gave the best cell viability (67.8%, Table S1). Therefore, we employed the combination of Liberase and DNase I for brain dissociation in all subsequent experiments.

To isolate the rare mural, endothelial, and microglial cell populations by FACS, we searched for cell surface proteins that are enriched in each of the cell types and screened for specific antibodies against these markers. We identified antibodies against PECAM1 (CD31) and CD102 that faithfully co-stained endothelial cells, as well as CD11b and CD45 antibodies that co-stained a microglial population (Figures 1A and 1B). We next searched for strongly expressed cell surface markers specific for the mural cell population. Utilizing a recently published single cell RNA sequencing dataset from the adult brain (Vanlandewijck et al., 2018), we chose to focus on *Pdgfrb* and *Cspg4* as they are both cell surface proteins and strongly expressed in all mural cells (Figures S1A–S1D). We screened antibodies against PDGFR β and CSPG4 through immunofluorescence and FACS analyses and were able to identify a highly specific PDGFR β antibody that we used in subsequent experiments (Figures 1C, 1D, and S1E–S1L).

The identity of individual cells can be determined via scRNA-seq through the analyses of cellular transcriptomes (Grun and van Oudenaarden, 2015). To test the specificity of our selected markers and antibodies, we stained E14.5 brain cells with the pre-screened antibodies, isolated them using FACS and determined cell identity through scRNA-seq with the mCEL-Seq2 protocol (Figure 1E). We defined neural cells using a

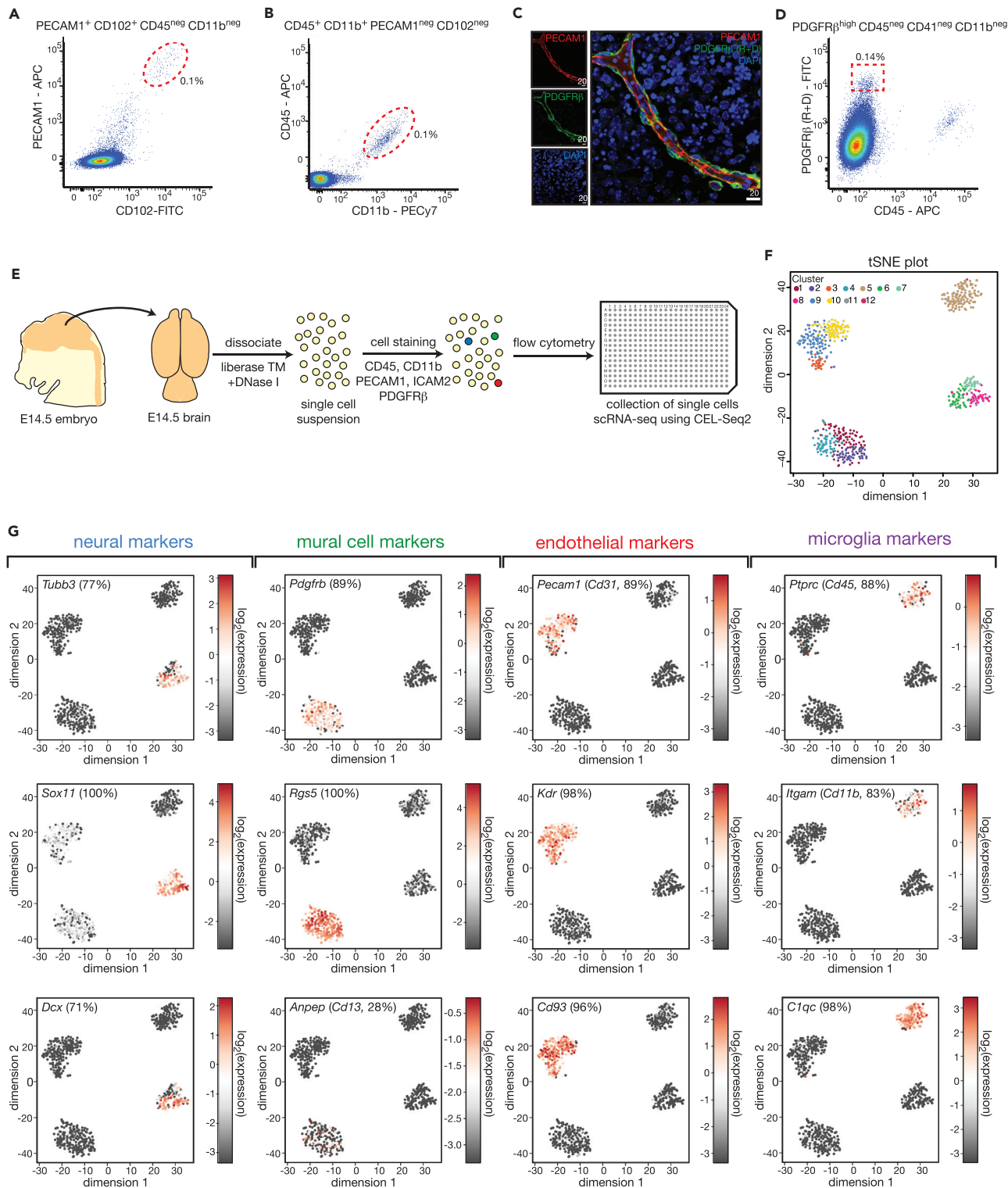


Figure 1. Identification of Cell Surface Markers for the Isolation of Neural, Microglial, and Vascular Cells

(A) FACS plot showing enrichment of endothelial cells using PECAM1 and CD102 (ICAM2).

(B) Exemplary FACS plot depicting the FACS strategy for the enrichment of microglia using CD11b and CD45.

Figure 1. Continued

(C) Immunofluorescence image showing a blood vessel in the E14.5 brain stained for the mural cell marker PDGFR β (green) and endothelial marker PECAM1 (red). The PDGFR β antibody (from R+D) showed high specificity as evident by the strong peri-vascular staining. This is in contrast to other tested PDGFR β and CSPG4 antibodies that showed unspecific staining (Figures S1H–S1L). Scale bars are provided in micrometers.

(D) Sorting strategy for PDGFR β -positive mural cells.

(E) Schematic representation of scRNA-seq procedure used to test the specificity of the neural, microglial, and vascular cell isolation procedure. E14.5 mouse brains were dissociated using Liberase and DNase I, and the single cell suspension stained for selected cell surface markers followed by FACS of single cells into 384-well plates. Libraries for sequencing were prepared using the mCEL-Seq2 protocol. Cells were isolated in equal numbers from three independent wild-type E14.5 brains.

(F) The t-distributed stochastic neighbor embedding (tSNE) plot generated with the RacelD3 package (Herman et al., 2018) of the 625 cells that were isolated using the selected cell surface markers and passed the filtering criteria (>1,500 unique transcripts). Twelve distinct clusters and four major cell populations were identified by unsupervised clustering.

(G) Expression of neural, mural, endothelial, and microglial cell-type-specific genes. Each of the cell types was confined to one of the major clusters. Note the low levels of Cd13 expression in the mural cell population. The numbers in parenthesis represent the proportion of cells in the respective cluster where marker expression was detectable.

See also Figures S1 and S2.

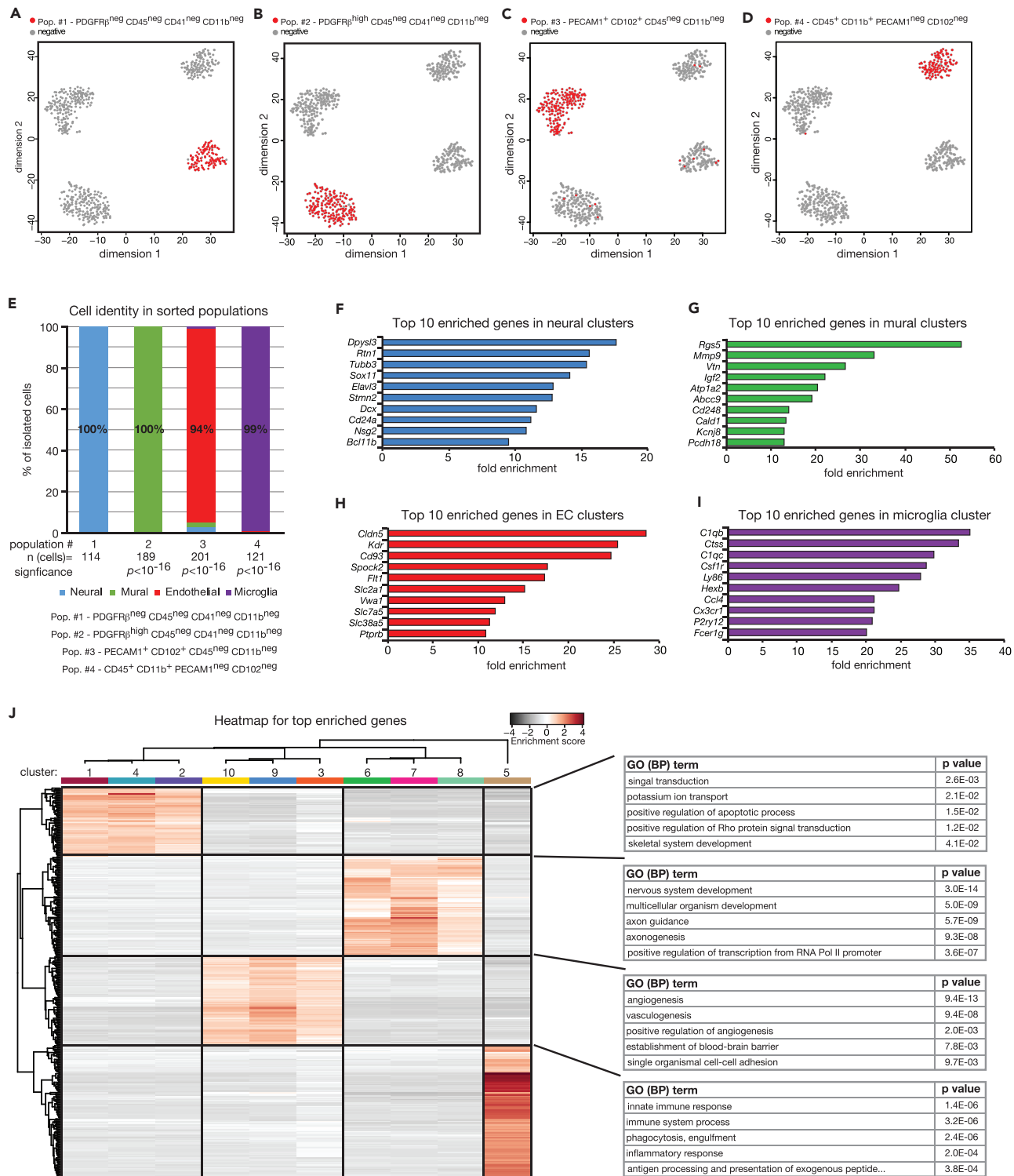
set of negative makers to ensure we were obtaining the full spectrum of neural cells present in the E14.5 brain (PECAM1 neg , CD102 neg , PDGFR β neg , CD45 neg , CD41 neg). Endothelial cells, mural cells, and microglia were selected based on positive markers as indicated in Figures 1A, 1B, and 1D. Following scRNA-seq, we filtered for cells with more than 1,500 transcripts, leading to the selection of 625 cells. Through unsupervised clustering of sorted cells using RacelD3 (Grun et al., 2015; Herman et al., 2018), we identified four major cell populations with 12 distinct clusters (Figure 1F). Each of the four major clusters specifically expressed markers of neural cells (*Tubb3*, *Sox11*, *Dcx*), mural cells (*Pdgfrb*, *Rgs5*, *Anpep*), endothelial cells (*Pecam1*, *Kdr*, *Cd93*), or microglia (*Ptprc*, *Itgam*, *C1qc*) (Figure 1G). We next correlated our selected cell surface markers to the identity of cells as determined by unsupervised clustering. We found that our selection criteria allowed us to isolate neural cells, mural cells, endothelial cells, and microglia to between 94% and 100% purity (Figures 2A–2E). Furthermore, each of the populations strongly expressed genes known to be important for their function (Figures 2F–2I, Tables S3–S6), whereas GO-term analyses showed significant enrichment of terms known to functionally correlate with each cell type (Figure 2J). Together, these analyses revealed that we were able to isolate the major cells within the developing brain, namely neural cells, mural cells, endothelial cells, and microglia, to high purity using a FACS-based strategy.

Identification of Heterogeneity in Neural, Mural, and Endothelial Cell Populations

We next wanted to examine the extent of cellular heterogeneity within each of the cell populations. To this end, we analyzed the clusters within each of the four major cell populations. Neural, mural, and endothelial cell populations contained three distinct clusters each, indicating heterogeneity within each cell type (Figure 1F). On the other hand, only one microglial cluster was detectable, probably because of the small number of cells sequenced (Figure 1F, cluster 5). We identified a number of characteristic genes for each subpopulation using differential gene expression analysis between the clusters (Figure S2). The greatest level of cellular heterogeneity was observed among the three neural clusters, reflecting the number of distinct neural stem and progenitor cells as well as distinct differentiating neurons found within the E14.5 brain (Figures S2A–S2D). Similarly, we detected three distinct cell states in the endothelial and mural cell clusters (Figures S2E–S2J), suggesting that our cell sorting procedure was indeed able to detect and isolate a range of neural, mural, and endothelial cell populations present in the mouse embryonic brain.

Simultaneous Isolation and Analyses of Neural, Mural, Endothelial, and Microglial Cells Using EMBRACE

Although scRNA-seq is an ideal tool for detecting cellular heterogeneity and phenotypic shifts in cell populations, only the most strongly expressed transcripts are typically detected. This may hinder the ability to detect the complete transcriptome of cells and undertake detailed analyses of functionally important lowly expressed genes and transcription factors. For this purpose, we simultaneously collected neural cells (CD45 neg , CD41 neg , CD11b neg , PECAM1 neg , CD102 neg , PDGFR β neg), mural cells (PDGFR β high , PECAM1 neg , CD102 neg , CD45 neg , CD41 neg , CD11b neg), endothelial cells (PECAM1 $^{+}$, CD102 $^{+}$, CD45 neg , CD41 neg , CD11b neg , PDGFR β neg), and microglia (CD45 medium , CD11b $^{+}$, PECAM1 neg , PDGFR β neg) from E14.5 brain samples by FACS using the markers that we had established (Figure 3A). We refer to this methodology as EMBRACE. Using EMBRACE, we obtained around 5.4 million neural cells, 4,000 mural cells, 4,000 endothelial cells, and 7,000 microglia from each E14.5 brain (Figure 3B). We analyzed the isolated cell population

**Figure 2. High Enrichment of Neural, Mural, Endothelial, and Microglial Cells Using EMBRACE**

(A–D) tSNE maps showing the clustering of cells sorted based on markers for (A) neural cells, (B) mural cells, (C) endothelial cells, and (D) microglia.

(E) Identity of cells in each of the four EMBRACE-sorted populations based on the comparison of cell surface markers and cell identity, as specified by unsupervised hierarchical clustering of scRNA-seq data.

(F–I) Top 10 genes enriched in (F) neural, (G) mural, (H) endothelial, and (I) microglia clusters. A more comprehensive list of genes enriched in each of the cell populations can be found in Tables S3–S6.

Figure 2. Continued

(J) Heatmap depicting mean expression per cluster of top enriched genes in each cell population together with gene ontology analysis (biological process). The enrichment score was calculated by determining the expression of a particular gene in a specific cell cluster relative to the mean expression of that same gene across all cell clusters.

See also Figure S2.

transcriptomes via RNA-seq. Compared with an average of 2,439 unique genes per cell in the single-cell RNA-seq experiments, we detected around 24,000 genes in the bulk population RNA-seq, giving us greater power for downstream analyses (Figure 3C). These observations were consistent with other scRNA-seq studies (Rosenberg et al., 2018; Vanlandewijck et al., 2018; Zeisel et al., 2018), which also detected between 677 and 3,254 unique genes per cell (Figure S3A). The EMBRACE-isolated cell populations were strongly enriched in their respective cell markers (Figure 3D and Tables S7–S10) and showed cell-type-appropriate biological functions in GO-term analyses (Figure 3E), thereby confirming their expected cell identities. Together, these analyses revealed that we could isolate highly enriched neural, mural, endothelial, and microglial cell populations via EMBRACE and detect a much richer transcriptome with bulk RNA-seq compared with scRNA-seq analyses.

Building a Cell-Cell Interaction Database

To uncover potential communication between neural, mural, endothelial, and microglial cells in the developing mouse brain, we built an *in silico* cell-cell communication network via quantification of ligand-receptor interactions between the four different cell types. We utilized the ligand-receptor pair dataset generated by Ramilowski and co-workers to identify cell-cell interactions (Ramilowski et al., 2015). We filtered the bulk RNA-seq data for genes that showed an average expression of greater than 10 FPKM across all four cell types. Consistent with the greater sensitivity of RNA-seq on bulk-sorted populations, we were able to identify 20-fold more cell-cell interactions in the bulk RNA-seq dataset compared with scRNA-seq data (Figures 4A and S3B–S3D). Indeed, our bioinformatics analyses predicted between 350 and 550 ligand-receptor interactions between each of the four different cell types with a total of 1,710 unique interactions based on the EMBRACE RNA-seq data, including extensive autocrine signaling (Figure 4B and Table S11). We have provided access to the complete inter-cellular communication database via the online “Brain interactome explorer” (<https://mpi-ie.shinyapps.io/braininteractomeexplorer/>).

We next wanted to test the accuracy of our database by interrogating the presence of well-established cell-cell interactions that are known to occur in the developing brain. VEGF-A from neural cells is known to induce the vascularization of the brain via angiogenesis (Haigh et al., 2003). Consistently, our analyses predicted a substantial interaction between *Vegfa* from neural cells with the VEGF receptor *Kdr* (*Vegfr2*) in endothelial cells (Figure 4C). Similarly, the interaction between the angiopoietin (*Angpt*) ligands and Tie receptors as well as between platelet-derived growth factors (PDGF) and PDGF receptors is critical for proper vascular development. We could indeed map strong interactions connecting these ligand-receptor pairs (Figures 4D and 4E). In addition, we searched for established communication modules essential for neural cell development. We uncovered widespread WNT and Ephrin signaling centered around neural cells (Figures S4B and S4C), consistent with the critical role of WNTs and Ephrins in neural development (Lisabeth et al., 2013; Mulligan and Cheyette, 2012; Noelanders and Vleminckx, 2017). Together, these examples suggest that our inter-cellular communication network is able to detect important inter-cellular communication modules known to occur in the E14.5 brain.

Having established that we could detect well-established cell-cell interactions in our dataset, we next focused on detecting potentially novel and previously overlooked communication modules within the developing brain. We mapped the interaction of the top 50 expressed ligand-receptor pairs, for which the ligand expression was enriched in at least one cell population (Figures 4F and S4D). Cells with the highest broadcasting capacity were microglia followed by mural cells. The strongest interactions were detected between microglia and neural cells and were underpinned by APOE signaling (Figures 4F and S4D). Although the importance of APOE signaling and APOE allele variants in Alzheimer disease is well established (Farrer et al., 1997; Poirier et al., 1993; Strittmatter et al., 1993), the importance of *Apoe* in development is comparatively poorly understood. Our transcriptomic analysis showed high levels of *Apoe* expression in microglia at E14.5 (Figure 5A). We confirmed the strong enrichment of APOE expression in IBA1⁺ microglia via immunofluorescence (Figure 5B). Consistent with the fact that APOE is a secreted protein (Bu, 2009), we also observed widespread APOE signal in the E14.5 brain (Figure 5B). We next tested

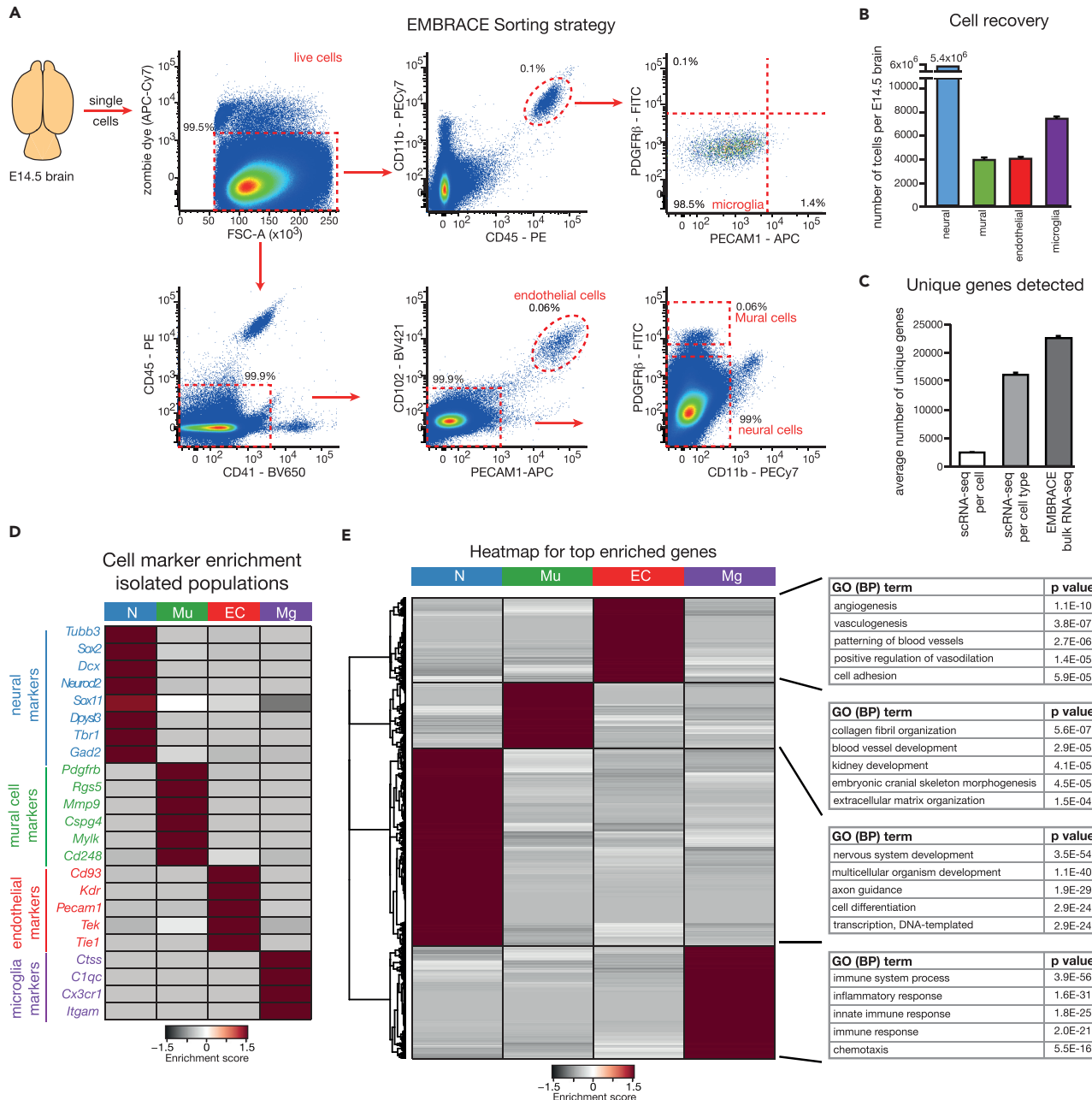


Figure 3. Population-Based Transcriptomic Analyses of Neural, Mural, Endothelial, and Microglial Cells Provide a Rich Cellular Transcriptome

(A) EMBRACE sorting strategy with representative gating for the isolation of neural cells, mural cells, endothelial cells, and microglia.

(B) Average numbers of cells recovered from each E14.5 brain. Error bars indicate mean \pm SEM. N = 6 E14.5 brains for neural cells and N = 11 E14.5 brains for endothelial, mural, and microglial cells.

(C) Mean number of unique genes detected per cell and per cell type in the scRNA-seq data, as well as in EMBRACE-based bulk RNA-seq experiments. Error bars indicate mean \pm SEM. N = 625 single cells isolated from three independent brains with a minimum of 1,500 unique transcripts; N = 3 wild-type brains for bulk population-based analyses.

(D) Enrichment of neural, mural, endothelial, and microglial markers in the four EMBRACE-enriched populations. A comprehensive list of genes enriched in each of the four populations is provided in Tables S7–S10.

(E) Gene ontology (biological processes) analyses of the top enriched genes (enrichment >10-fold) in each of the four EMBRACE-isolated cell populations — neural, mural, endothelial, and microglial cells.

The enrichment scores in (D) and (E) were calculated by determining the expression of a particular gene in a specific cell type relative to the mean expression of that same gene across all 4 EMBRACE-isolated cell populations.

EC - endothelial cells; Mg - microglia; Mu - mural cells; N - neural cells. See also Figure S3.

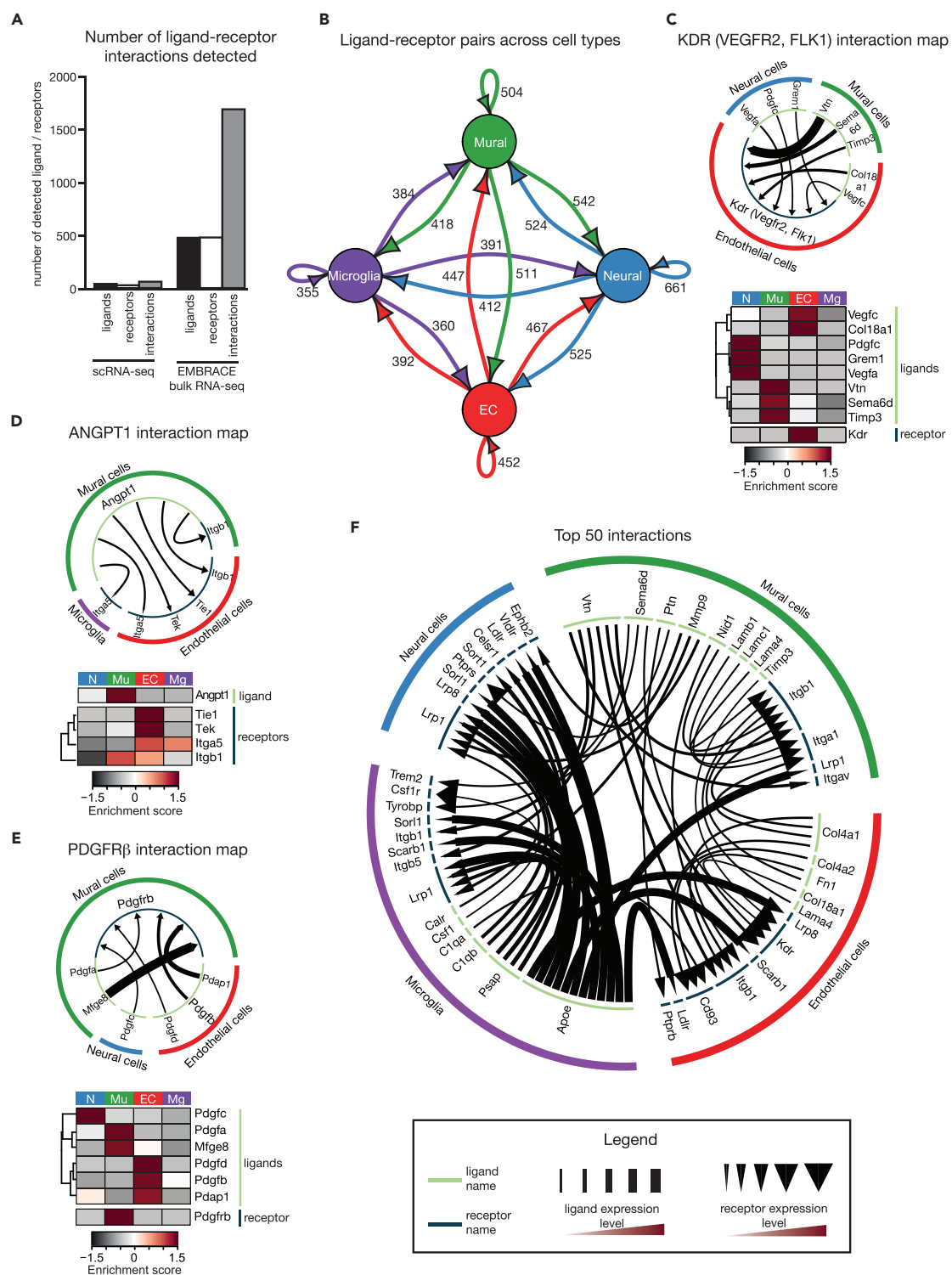


Figure 4. Extensive Inter-Cellular Communication in the Developing Brain

(A) Number of detected ligands, receptors, and ligand-receptor pairs in the scRNA-seq dataset compared with transcriptional analyses of bulk isolated cell populations.

(B) Map of ligand and receptor interactions between neural, mural, endothelial, and microglial cells based on transcriptomic analyses of EMBRACE-isolated cell populations. Arrow color corresponds to the ligand source, and the numbers indicate the quantity of detected ligand-receptor pairs between the indicated cell types. The comparable interaction map for the scRNA-seq data is provided in Figure S3B.

Figure 4. Continued

(C) Interaction map of the KDR (VEGFR2, FLK1) receptor network. Expression of *Kdr* is confined to endothelial cells, whereas its ligands are expressed by neural, mural, and endothelial cells. The heatmap represents the enrichment of gene expression in the four different cell types.

(D) Interaction map and associated heatmap for the ligand ANGPT1 (Angiopoietin). *Angpt1* is expressed only in mural cells and has corresponding receptors in microglia and endothelial cells.

(E) Interaction map and corresponding heatmap of the PDGFR β receptor network.

(F) Top 50 strongest predicted interactions between neural, mural, endothelial, and microglia cells. This list was generated by ranking the absolute expression levels of ligand-receptor pairs across the four cell types and filtering for ligands showing cell-type specific expression. The associated heatmap is provided in Figure S4D.

The enrichment score was calculated by determining the expression of a particular gene in a specific cell type relative to the mean expression of that same gene across all four EMBRACE-isolated cell populations. EC – endothelial cells, Mg – microglia, Mu – mural cells, N – neural cells. See also Figures S3 and S4.

whether APOE could interact with its known receptors LRP1 and LDLR in the E14.5 brain. Through immunofluorescence, we found the APOE expression pattern to overlap with LRP1 and LDLR signals (Figures 5C, 5D, and S4E). In addition, immunoprecipitation of endogenous APOE was able to pull down LRP1 in lysates of the E14.5 brain (Figure 5E), highlighting the existence of significant APOE signaling activity in the developing brain. These data suggest that microglia-expressed APOE is likely to have an important role in brain development through its extensive signaling to embryonic neural and endothelial cells.

Mural cells showed strong expression of secreted proteins that are not well studied in the context of neural development. The most prominent was vitronectin (*Vtn*), which is thought to signal via integrins as well as KDR (Murphy and Stupack, 2010; Wang et al., 2015). Consistent with previous work (Seiffert et al., 1995), we observed that *VTN* expression is confined to mural cells in the E14.5 brain (Figure 5F, left panel and S4D). The significance of these observations is currently unknown. Nevertheless, work in human umbilical cord vascular endothelial cells (HUVEC) has suggested that glycated VTN is able to inhibit the KDR receptor as well as the outgrowth and migration of endothelial cells (Wang et al., 2015). Consistently, our analyses suggest strong *Vtn* signaling from mural cells to *Kdr* in endothelial cells (Figure 5F). We were able to confirm the endothelial-specific expression of KDR as well as the interaction between VTN and KDR in the E14.5 brain using immunofluorescence analyses (Figures 5F and 5G). Although the importance of this communication module in the developing brain is yet to be established, this interaction is consistent with the role of mural cells in controlling aspects of endothelial cell development.

Mural cells also strongly expressed pleiotrophin (*Ptn*), a peptide showing high expression during development and in diseased states (Li et al., 1990; Poulsen et al., 2000; Takeda et al., 1995; Yeh et al., 1998). PTN can signal through a multitude of receptors, including integrins, N-syndecan, and receptor protein tyrosine phosphatases (PTPR) (Gonzalez-Castillo et al., 2014). In neural injury models, PTN is strongly upregulated and acts in a neuro-protective manner while promoting outgrowth of neurites (Mi et al., 2007). The precise contribution of PTN during the developmental time frame remains unknown. However, it is likely to play an important role given that *Ptn* knockout animals display neurological symptoms including increased anxiety, reduced social interaction, and a reduction in layer IV of the cortex (Krellman et al., 2014).

The most prominent ligands expressed by endothelial cells were non-canonical ligands of extracellular matrix proteins, including collagens and laminin subunit A4 (*Lama4*), which act primarily on endothelial cells as well as mural cells (Figure 4F). LAMA4 is found in the extracellular matrix surrounding endothelial cells and binds to integrin β 1 (ITGB1) (Gonzalez et al., 2002). In the context of the E14.5 brain, *Itgb1* displayed the highest expression in mural cells, whereas LAMA4 was most strongly expressed in endothelial cells (Figure 5H). We found a strong overlap between LAMA4 and ITGB1 protein expression in immunofluorescence stainings (Figure 5I). Although *Lama4* deletion is known to cause defects in angiogenesis (Stenzel et al., 2011), the importance of the cross talk between endothelial LAMA4 and mural cell ITGB1 during neural vasculature development remains unclear.

Together, these examples highlight the versatility of our approach in facilitating the identification of potentially new and under-appreciated inter-cellular communication modules within the developing brain.

DISCUSSION

In the current study, we set out to establish a method for the simultaneous isolation of neural, mural, endothelial, and microglial cells and subsequently apply this method to map the cell-cell communication networks that exist in the developing mouse brain. We show here that we could enrich each of the four cell

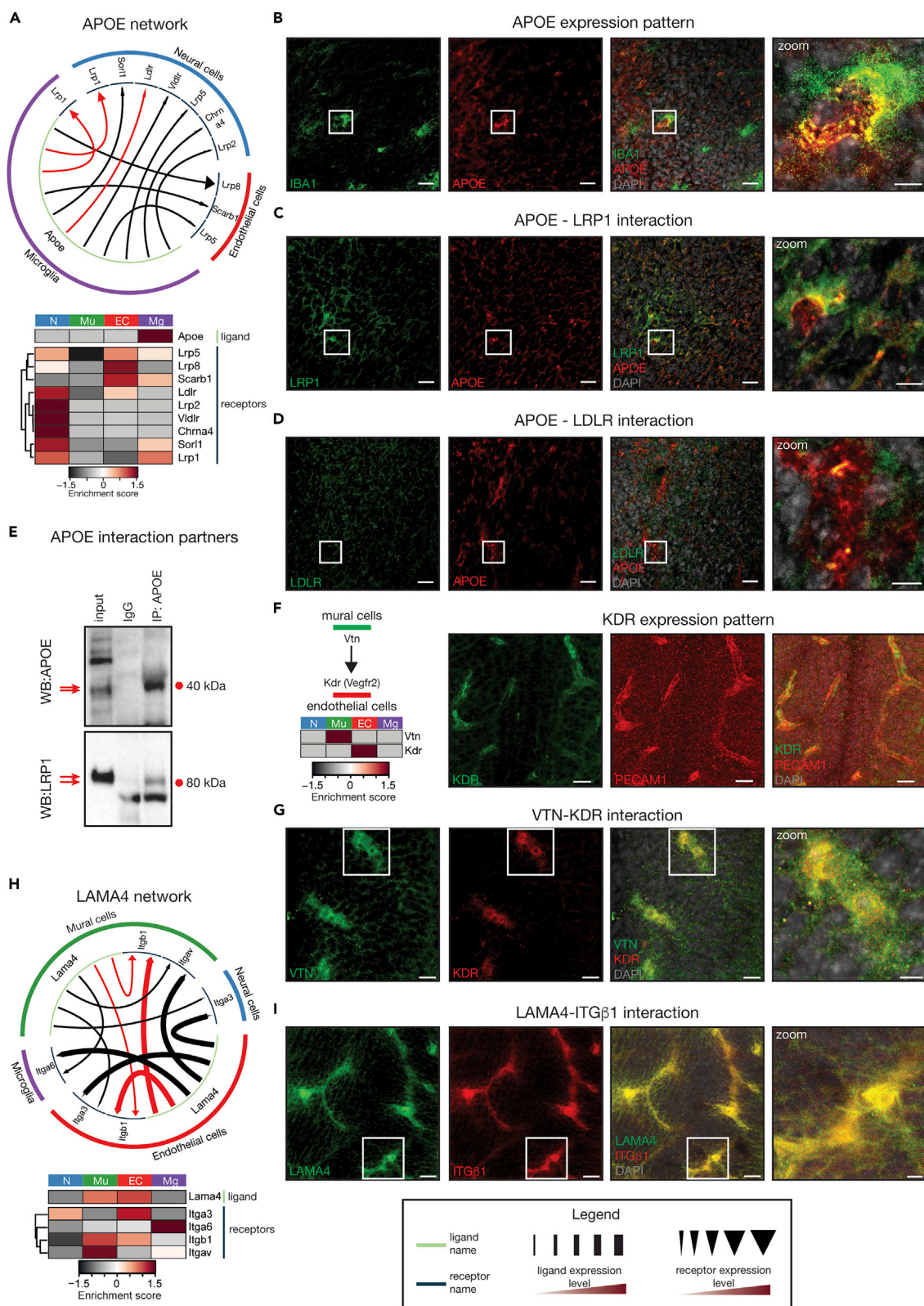


Figure 5. Confirmation of Inter-Cellular Signaling Modules

- (A) Interaction map of the apolipoprotein E (APOE) network. Apoe is strongly expressed in microglia, whereas its receptors are primarily enriched in endothelial and neural cells. The heatmap displays enrichment in gene expression of Apoe and its receptors in the different cell populations. Red lines indicate the predicted APOE–LDLR and the APOE–LRP1 interactions that were experimentally tested.
- (B) Enrichment of APOE protein expression in IBA1-positive microglia in the E14.5 brain. Scale bars are 20 μm in the first three panels and 5 μm in the zoom panel.
- (C) Immunofluorescence imaging showing overlap of APOE (red) and LRP1 (green) proteins in the E14.5 brain. Scale bars represent 20 μm in the first three panels and 5 μm in the zoom panel.
- (D) Immunofluorescence showing overlap of APOE (red) and LDLR (green) proteins in sections of the E14.5 brain. Scale bars represent 20 μm in the first three panels and 5 μm in the zoom panel.
- (E) Co-immunoprecipitation assay showing direct protein interaction between APOE and LRP1. APOE was immunoprecipitated from E14.5 brain lysates and the IP material was subsequently probed with APOE and LRP1 antibodies via western blot analysis.
- (F) Diagram showing the expected interaction between VTN and KDR. The full KDR interaction network is provided in Figure 4C. The immunofluorescence images show the expected enrichment of KDR protein expression in PECAM1-positive endothelial cells. Scale bars indicate 20 μm.
- (G) Immunofluorescence imaging of E14.5 brain sections showing overlap between vitronectin (VTN, green) and KDR (red) protein expression. Scale bars indicate 10 μm in the first three panels and 5 μm in the zoom image.
- (H) Interaction map and corresponding heatmap of the LAMA4 network. The LAMA4 and ITGB1 interaction, highlighted in red, was tested by immunofluorescence analyses.
- (I) Immunofluorescence images showing overlap between LAMA4 (green) and ITGβ1 (red) proteins in the E14.5 brain. Scale bars indicate 20 μm in the first three panels and 5 μm in the zoom image.
- The enrichment score was calculated by determining the expression of a particular gene in a specific cell type relative to the mean expression of that same gene across all four EMBRACE-isolated cell populations.
- EC - endothelial cells; IP - immunoprecipitation; Mg - microglia; Mu - mural cells; N - neural cells; WB - western blot. See also Figure S4.

populations to more than 94% purity using EMBRACE. Undertaking a direct comparison of single cell and bulk FACS-purified transcriptomes, we show that around 20-fold more ligand-receptor pairs are detectable in the bulk FACS-purified populations. Using an *in silico* approach, we map the cell-cell communication networks and chart the E14.5 brain interactome, revealing extensive communication between neural, mural, endothelial, and microglial cells. We experimentally confirmed selected interactions from the top 50 list, including APOE-LRP1, APOE-LDLR, VTN-KDR, and LAMA4-ITGβ1, emphasizing the biological relevance of our database.

Since cells *in vivo* are present in a complex environment, it is important to study gene function in specific cell types in the context of the whole organ or even the organism. Using single cell or nucleus RNA-seq analysis, inter-cellular communication databases have been generated for the heart (Skelly et al., 2018), kidney (Wu et al., 2019), liver organoids (Camp et al., 2017), as well as tumors isolated from mouse models (Kumar et al., 2018) and human patients (Puram et al., 2017; Zhou et al., 2017). Although single cell RNA-seq is powerful in the identification of rare cell types and detection of heterogeneity between similar cell populations, bulk RNA-seq analyses on cell populations provides a much richer transcriptome. Thus, using a combination of both scRNA-seq and bulk population-based RNA-seq provides a much more comprehensive picture of cell function compared with either technique alone. The disadvantage of a population-based RNA-seq approach is the time-consuming task of identifying and verifying cell-type specific markers that are critical for the isolation of near-pure cell populations. In contrast, cell identity can be retrospectively assigned in scRNA-seq datasets based on the cellular transcriptome. However, not all genomic techniques are currently amenable to single cell technologies and require the isolation of larger cell populations. To this end, we have established EMBRACE, a method to simultaneously isolate neural, mural, endothelial, and microglial cells to high purity. This sorting methodology will be particularly useful to researchers conducting experiments that are not yet compatible with single cell analyses, such as 3D chromatin conformation capture or chromatin immunoprecipitation (ChIP). Furthermore, given the simplicity of EMBRACE, it can easily be applied to study cell-cell communication in cell-type specific knockout mouse models.

In contrast to EMBRACE, more complex techniques have been applied to isolate different cell types from the adult mouse brain. Through immunopanning, transgenic animal models, as well as FACS, Zhang and co-workers have enriched and transcriptionally analyzed endothelial cells, microglia, progenitor and mature oligodendrocytes, neurons, and astrocytes (Zhang et al., 2014, 2016) and reported significant differences in transcriptional splicing between these cell types (Zhang et al., 2014). Although it is difficult to ascertain whether all cellular subtypes survive the purification procedure, these datasets nevertheless provide an excellent resource for exploring the transcriptional complexity of cell types in the adult brain. In

contrast, we have focused here on the embryonic brain to determine inter-cellular communication modules that are likely important for neural development. We identified a total of 1,710 interactions, many of which are likely to play an important role during development (Figure 4B and Table S11, <https://mpi-ie.shinyapps.io/braininteractomeexplorer/>).

Among the strongest interactions, we found microglia-expressed *Apoe* to mediate communication with neural, endothelial, and mural cells in the E14.5 brain (Figures 4F and 5A–5E). APOE is highly abundant in the brain and is involved in lipid transport, clearance of lipoproteins, and cholesterol homeostasis (Hauser et al., 2011; Huang and Mahley, 2014). *Apoe* knockout mice kept on a high-fat diet show significant accumulation of lipids in the brain (Walker et al., 1997). At least in mouse models, APOE cannot cross the BBB (Liu et al., 2012) and must therefore be produced locally. Our analyses show that microglia are the major producers of APOE in the E14.5 brain (Figures 5A and 5B). There are some indications that APOE may be important in brain development. The APOE e4 allele variant is the best-known genetic risk factor associated with Alzheimer disease (Farrer et al., 1997; Poirier et al., 1993; Strittmatter et al., 1993), and infants carrying this variant show delayed myelination and gray matter development in brain regions typically affected by Alzheimer disease (Dean et al., 2014). In addition to extensive signaling between microglia-derived APOE and neural cells, our analyses revealed interactions between APOE and its reported receptors in vascular cells (Figure 4F). These interactions are also likely to be important during development, as mice lacking *Apoe* display increased permeability of neural vasculature but not of vessels from other organs (Hafezi-Moghadam et al., 2007; Methia et al., 2001). It is currently unknown which molecular mechanisms drive this specific defect in neural vasculature and how *Apoe* deficiency impacts neural vascular function. Together with our cell-cell interactome, these studies highlight the potential importance of APOE during the developmental time frame and encourage the investigation of APOE during early brain development. In addition to APOE, our dataset provides a resource of 1,710 total inter-cellular interactions that are likely to play important roles during the neural developmental time frame.

In summary, we describe here EMBRACE, a method to simultaneously isolate neural, mural, endothelial, and microglial cells to high purity. This simple method will allow researchers to explore inter-cellular interactions in their mouse models of choice. Using EMBRACE, we isolated, transcriptionally analyzed, and built an inter-cellular communication network in the E14.5 brain that revealed 1,710 unique ligand-receptor relationships (<https://mpi-ie.shinyapps.io/braininteractomeexplorer/>). Our dataset and brain communication network underlie the richness of inter-cellular communication present in the developing brain and provide a comprehensive resource that will allow the field to dissect the importance of selected receptors and ligands in the context of neural development.

Limitations of the Study

In the current study, we establish the EMBRACE methodology that we use to analyze inter-cellular communication in the developing mouse brain. Given the complexity of adult brains, which consist of extensive neural processes that are prone to damage during dissociation, the EMBRACE procedure may not be successful in isolating neural cells from the adult brain. However, EMBRACE is still likely to be efficient in isolating endothelial, mural, and microglial cells from the adult brain, as they express the same cell surface markers as their embryonic counterparts and are resistant to harsh dissociation regimens.

Using the EMBRACE technique, we isolated neural, mural, endothelial, and microglial cells from the E14.5 brain and built an inter-cellular interactome based on the transcriptional profiles of each cell type. Our database is built on gene expression levels in neural, mural, endothelial, and mural cells and uses a collated list of ligand-receptor interactions (Ramilowski et al., 2015), which is based on diverse cell types. Thus, it will be prudent for researchers to experimentally confirm their interactions of interest in a similar fashion as we have done for APOE-LDLR, APOE-LRP1, VTN-KDR, and LAMA4-ITGB1 in the E14.5 brain.

METHODS

All methods can be found in the accompanying [Transparent Methods supplemental file](#).

DATA AND CODE AVAILABILITY

The Brain Interactome Explorer is available at <https://mpi-ie.shinyapps.io/braininteractomeexplorer/>.

Raw sequencing data have been uploaded to GEO and are available under GSE133079.

SUPPLEMENTAL INFORMATION

Supplemental Information can be found online at <https://doi.org/10.1016/j.isci.2019.10.026>.

ACKNOWLEDGMENTS

We thank Thomas Manke, Maria Shvedunova, and Cecilia Pessoa for helpful discussions and critical reading of the manuscript. We are grateful to the MPI flow cytometry facility, MPI sequencing facility, and MPI animal house for technical assistance. We thank Omar Mossad for the provision of the ITB β 1 antibody and Anne Drougard for the IBA1 antibody. This work was supported by the Alexander von Humboldt Foundation (in support of B.N.S.), DFG grant GR4980/3-1, the Behrens-Weise-Foundation (in support of S.), and the CRC992 (in support of A.A., L.H., and O.B.), CRC746 and CRC1140 (in support of A.A.) grants. This work was further supported by CRC1381 (Project-ID 403222702).

AUTHOR CONTRIBUTIONS

B.N.S. and A.A. conceived the project. B.N.S., O.B., S.G., T.H.T., S., N.A., and H.H. undertook the experiments. K.S. prepared the brain interactome website. B.N.S., O.B., T.H.T., S.G., and N.A. undertook the analyses. B.N.S., O.B., and A.A. wrote the paper. A.A., B.N.S., L.H., and D.G. supervised the project. All authors edited and approved the manuscript.

DECLARATION OF INTERESTS

The authors declare no conflict of interest.

Received: May 25, 2019

Revised: September 24, 2019

Accepted: October 13, 2019

Published: November 22, 2019

REFERENCES

- Alliot, F., Godin, I., and Pessac, B. (1999). Microglia derive from progenitors, originating from the yolk sac, and which proliferate in the brain. *Brain Res. Dev. Brain Res.* 117, 145–152.
- Barnabe-Heider, F., Wasylka, J.A., Fernandes, K.J., Porsche, C., Sendtner, M., Kaplan, D.R., and Miller, F.D. (2005). Evidence that embryonic neurons regulate the onset of cortical gliogenesis via cardiotrophin-1. *Neuron* 48, 253–265.
- Bennett, M.L., Bennett, F.C., Liddelow, S.A., Ajami, B., Zamanian, J.L., Fernhoff, N.B., Mulinyawe, S.B., Bohlen, C.J., Adil, A., Tucker, A., et al. (2016). New tools for studying microglia in the mouse and human CNS. *Proc. Natl. Acad. Sci. U S A* 113, E1738–E1746.
- Bu, G. (2009). Apolipoprotein E and its receptors in Alzheimer's disease: pathways, pathogenesis and therapy. *Nat. Rev. Neurosci.* 10, 333–344.
- Camp, J.G., Sekine, K., Gerber, T., Loeffler-Wirth, H., Binder, H., Gac, M., Kanton, S., Kageyama, J., Damm, G., Seehofer, D., et al. (2017). Multilineage communication regulates human liver bud development from pluripotency. *Nature* 546, 533–538.
- Crouch, E.E., and Doetsch, F. (2018). FACS isolation of endothelial cells and pericytes from mouse brain microregions. *Nat. Protoc.* 13, 738–751.
- Crouch, E.E., Liu, C., Silva-Vargas, V., and Doetsch, F. (2015). Regional and stage-specific effects of prospectively purified vascular cells on the adult V-SVZ neural stem cell lineage. *J. Neurosci.* 35, 4528–4539.
- Czupalla, C.J., Yousef, H., Wyss-Coray, T., and Butcher, E.C. (2018). Collagenase-based single cell isolation of primary murine brain endothelial cells using flow cytometry. *Bio. Protoc.* 8, e3092.
- Daneman, R., Zhou, L., Agalliu, D., Cahoy, J.D., Kaushal, A., and Barres, B.A. (2010a). The mouse blood-brain barrier transcriptome: a new resource for understanding the development and function of brain endothelial cells. *PLoS One* 5, e13741.
- Daneman, R., Zhou, L., Kebede, A.A., and Barres, B.A. (2010b). Pericytes are required for blood-brain barrier integrity during embryogenesis. *Nature* 468, 562–566.
- Datta, M., Staszewski, O., Raschi, E., Frosch, M., Hagemeyer, N., Tay, T.L., Blank, T., Kreutzfeldt, M., Merkler, D., Ziegler-Waldkirch, S., et al. (2018). Histone deacetylases 1 and 2 regulate microglia function during development, homeostasis, and neurodegeneration in a context-dependent manner. *Immunity* 48, 514–529.e6.
- Dean, D.C., 3rd, Jerskey, B.A., Chen, K., Protas, H., Thiyyagura, P., Roontiva, A., O'Muircheartaigh, J., Dirks, H., Waskiewicz, N., Lehman, K., et al. (2014). Brain differences in infants at differential genetic risk for late-onset Alzheimer disease: a cross-sectional imaging study. *JAMA Neurol.* 71, 11–22.
- Epshtain, A., Rachi, E., Sakhneny, L., Mizrahi, S., Baer, D., and Landsman, L. (2017). Neonatal pancreatic pericytes support beta-cell proliferation. *Mol. Metab.* 6, 1330–1338.
- Fan, J., Ponferrada, V.G., Sato, T., Vemaraju, S., Fruttiger, M., Gerhardt, H., Ferrara, N., and Lang, R.A. (2014). Crim1 maintains retinal vascular stability during development by regulating endothelial cell Vegfa autocrine signaling. *Development* 141, 448–459.
- Farrer, L.A., Cupples, L.A., Haines, J.L., Hyman, B., Kukull, W.A., Mayeux, R., Myers, R.H., Pericak-Vance, M.A., Risch, N., and van Duijn, C.M. (1997). Effects of age, sex, and ethnicity on the association between apolipoprotein E genotype and Alzheimer disease. A meta-analysis. APOE and Alzheimer Disease Meta Analysis Consortium. *JAMA* 278, 1349–1356.
- Gonzalez, A.M., Gonzales, M., Herron, G.S., Nagavarapu, U., Hopkinson, S.B., Tsuruta, D., and Jones, J.C. (2002). Complex interactions between the laminin alpha 4 subunit and integrins regulate endothelial cell behavior in vitro and angiogenesis in vivo. *Proc. Natl. Acad. Sci. U S A* 99, 16075–16080.
- Gonzalez-Castillo, C., Ortuno-Sahagun, D., Guzman-Brambila, C., Pallas, M., and

- Rojas-Mayorquin, A.E. (2014). Pleiotrophin as a central nervous system neuromodulator, evidences from the hippocampus. *Front. Cell. Neurosci.* 8, 443.
- Grun, D., and van Oudenaarden, A. (2015). Design and analysis of single-cell sequencing experiments. *Cell* 163, 799–810.
- Grun, D., Lyubimova, A., Kester, L., Wiebrands, K., Basak, O., Sasaki, N., Clevers, H., and van Oudenaarden, A. (2015). Single-cell messenger RNA sequencing reveals rare intestinal cell types. *Nature* 525, 251–255.
- Hafezi-Moghadam, A., Thomas, K.L., and Wagner, D.D. (2007). ApoE deficiency leads to a progressive age-dependent blood-brain barrier leakage. *Am. J. Physiol. Cell Physiol.* 292, C1256–C1262.
- Haigh, J.J., Morelli, P.I., Gerhardt, H., Haigh, K., Tsien, J., Damert, A., Miquerol, L., Muhlnier, U., Klein, R., Ferrara, N., et al. (2003). Cortical and retinal defects caused by dosage-dependent reductions in VEGF-A paracrine signaling. *Dev. Biol.* 262, 225–241.
- Hauser, P.S., Narayanaswami, V., and Ryan, R.O. (2011). Apolipoprotein E: from lipid transport to neurobiology. *Prog. Lipid Res.* 50, 62–74.
- He, L., Vanlandewijck, M., Raschperger, E., Andaloussi Mae, M., Jung, B., Lebouvier, T., Ando, K., Hofmann, J., Keller, A., and Betsholtz, C. (2016). Analysis of the brain mural cell transcriptome. *Sci. Rep.* 6, 35108.
- Hellstrom, M., Kalen, M., Lindahl, P., Abramsson, A., and Betsholtz, C. (1999). Role of PDGF-B and PDGFR-beta in recruitment of vascular smooth muscle cells and pericytes during embryonic blood vessel formation in the mouse. *Development* 126, 3047–3055.
- Herman, J.S., Sagar, and Grun, D. (2018). Fatel infers cell fate bias in multipotent progenitors from single-cell RNA-seq data. *Nat. Methods* 15, 379–386.
- Huang, Y., and Mahley, R.W. (2014). Apolipoprotein E: structure and function in lipid metabolism, neurobiology, and Alzheimer's diseases. *Neurobiol. Dis.* 72 (Pt A), 3–12.
- Jiang, X., and Nardelli, J. (2016). Cellular and molecular introduction to brain development. *Neurobiol. Dis.* 92, 3–17.
- Krellman, J.W., Ruiz, H.H., Marciano, V.A., Mondrow, B., and Croll, S.D. (2014). Behavioral and neuroanatomical abnormalities in pleiotrophin knockout mice. *PLoS One* 9, e100597.
- Kumar, M.P., Du, J., Lagoudas, G., Jiao, Y., Sawyer, A., Drummond, D.C., Lauffenburger, D.A., and Ruea, A. (2018). Analysis of single-cell RNA-seq identifies cell-cell communication associated with tumor characteristics. *Cell Rep.* 25, 1458–1468.e4.
- Li, Y.S., Milner, P.G., Chauhan, A.K., Watson, M.A., Hoffman, R.M., Kodner, C.M., Milbrandt, J., and Deuel, T.F. (1990). Cloning and expression of a developmentally regulated protein that induces mitogenic and neurite outgrowth activity. *Science* 250, 1690–1694.
- Lisabeth, E.M., Falivelli, G., and Pasquale, E.B. (2013). Eph receptor signaling and ephrins. *Cold Spring Harb. Perspect. Biol.* 5, a009159.
- Liu, M., Kuhel, D.G., Shen, L., Hui, D.Y., and Woods, S.C. (2012). Apolipoprotein E does not cross the blood-cerebrospinal fluid barrier, as revealed by an improved technique for sampling CSF from mice. *Am. J. Physiol. Regul. Integr. Comp. Physiol.* 303, R903–R908.
- Ma, S., Santhosh, D., Kumar, T.P., and Huang, Z. (2017). A brain-region-specific neural pathway regulating germinal matrix angiogenesis. *Dev. Cell* 41, 366–381.e4.
- Matcovitch-Natan, O., Winter, D.R., Giladi, A., Vargas Aguilar, S., Spindrad, A., Sarrazin, S., Ben-Yehuda, H., David, E., Zelada Gonzalez, F., Perrin, P., et al. (2016). Microglia development follows a stepwise program to regulate brain homeostasis. *Science* 353, aad8670.
- Mathys, H., Adaikkan, C., Gao, F., Young, J.Z., Manet, E., Hemberg, M., De Jager, P.L., Ransohoff, R.M., Regev, A., and Tsai, L.H. (2017). Temporal tracking of microglia activation in neurodegeneration at single-cell resolution. *Cell Rep.* 21, 366–380.
- Methia, N., Andre, P., Hafezi-Moghadam, A., Economopoulos, M., Thomas, K.L., and Wagner, D.D. (2001). ApoE deficiency compromises the blood brain barrier especially after injury. *Mol. Med.* 7, 810–815.
- Mi, R., Chen, W., and Hoke, A. (2007). Pleiotrophin is a neurotrophic factor for spinal motor neurons. *Proc. Natl. Acad. Sci. U S A* 104, 4664–4669.
- Mulligan, K.A., and Cheyette, B.N. (2012). Wnt signaling in vertebrate neural development and function. *J. Neuroimmune Pharmacol.* 7, 774–787.
- Murphy, E., and Stupack, D. (2010). Vitronectin-Binding integrins in cancer. In *Cell-Extracellular Matrix Interactions in Cancer*, R. Zent and A. Pozzi, eds. (Springer), pp. 137–170.
- Nikolakopoulou, A.M., Dutta, R., Chen, Z., Miller, R.H., and Trapp, B.D. (2013). Activated microglia enhance neurogenesis via trypsinogen secretion. *Proc. Natl. Acad. Sci. U S A* 110, 8714–8719.
- Noelanders, R., and Vleminckx, K. (2017). How Wnt signaling builds the brain: bridging development and disease. *Neuroscientist* 23, 314–329.
- Paolicelli, R.C., Bolasco, G., Pagani, F., Maggi, L., Scianni, M., Panzanelli, P., Giustetto, M., Ferreira, T.A., Guiducci, E., Dumas, L., et al. (2011). Synaptic pruning by microglia is necessary for normal brain development. *Science* 333, 1456–1458.
- Poirier, J., Davignon, J., Bouthillier, D., Kogan, S., Bertrand, P., and Gauthier, S. (1993). Apolipoprotein E polymorphism and Alzheimer's disease. *Lancet* 342, 697–699.
- Poulsen, F.R., Lagord, C., Courty, J., Pedersen, E.B., Barrault, D., and Finsen, B. (2000). Increased synthesis of heparin affin regulatory peptide in the perforant path lesioned mouse hippocampal formation. *Exp. Brain Res.* 135, 319–330.
- Puram, S.V., Tirosh, I., Parikh, A.S., Patel, A.P., Yizhak, K., Gillespie, S., Rodman, C., Luo, C.L., Mroz, E.A., Emerick, K.S., et al. (2017). Single-cell transcriptomic analysis of primary and metastatic tumor ecosystems in head and neck cancer. *Cell* 171, 1611–1624.e24.
- Ramilowski, J.A., Goldberg, T., Harshbarger, J., Kloppmann, E., Lizio, M., Satagopam, V.P., Itoh, M., Kawaji, H., Carninci, P., Rost, B., et al. (2015). A draft network of ligand-receptor-mediated multicellular signalling in human. *Nat. Commun.* 6, 7866.
- Rosenberg, A.B., Roco, C.M., Muscat, R.A., Kuchina, A., Sample, P., Yao, Z., Graybuck, L.T., Peeler, D.J., Mukherjee, S., Chen, W., et al. (2018). Single-cell profiling of the developing mouse brain and spinal cord with split-pool barcoding. *Science* 360, 176–182.
- Seiffert, D., Iruela-Arispe, M.L., Sage, E.H., and Loskutoff, D.J. (1995). Distribution of vitronectin mRNA during murine development. *Dev. Dyn.* 203, 71–79.
- Sellner, S., Paricio-Montesinos, R., Spiess, A., Masuch, A., Erny, D., Harsan, L.A., Elverfeldt, D.V., Schwabenland, M., Biber, K., Staszewski, O., et al. (2016). Microglial CX3CR1 promotes adult neurogenesis by inhibiting Sirt 1/p65 signaling independent of CX3CL1. *Acta Neuropathol. Commun.* 4, 102.
- Sengillo, J.D., Winkler, E.A., Walker, C.T., Sullivan, J.S., Johnson, M., and Zlokovic, B.V. (2013). Deficiency in mural vascular cells coincides with blood-brain barrier disruption in Alzheimer's disease. *Brain Pathol.* 23, 303–310.
- Skelly, D.A., Squiers, G.T., McLellan, M.A., Bolisetty, M.T., Robson, P., Rosenthal, N.A., and Pinto, A.R. (2018). Single-cell transcriptional profiling reveals cellular diversity and intercommunication in the mouse heart. *Cell Rep.* 22, 600–610.
- Stenzel, D., Franco, C.A., Estrach, S., Mettouchi, A., Sauvaget, D., Rosewell, I., Schertel, A., Armer, H., Domogatskaya, A., Rodin, S., et al. (2011). Endothelial basement membrane limits tip cell formation by inducing DLL4/Notch signalling in vivo. *EMBO Rep.* 12, 1135–1143.
- Stremmel, C., Schuchert, R., Wagner, F., Thaler, R., Weinberger, T., Pick, R., Mass, E., Ishikawa-Ankerhold, H.C., Margraf, A., Hutter, S., et al. (2018). Yolk sac macrophage progenitors traffic to the embryo during defined stages of development. *Nat. Commun.* 9, 75.
- Strittmatter, W.J., Saunders, A.M., Schmechel, D., Pericak-Vance, M., Enghild, J., Salvesen, G.S., and Roses, A.D. (1993). Apolipoprotein E: high-affinity binding to beta-amyloid and increased frequency of type 4 allele in late-onset familial Alzheimer disease. *Proc. Natl. Acad. Sci. U S A* 90, 1977–1981.
- Takeda, A., Onodera, H., Sugimoto, A., Itoyama, Y., Kogure, K., Rauvala, H., and Shibahara, S. (1995). Induction of heparin-binding growth-associated molecule expression in reactive astrocytes following hippocampal neuronal injury. *Neuroscience* 68, 57–64.
- Tata, M., Ruhrberg, C., and Fantin, A. (2015). Vascularisation of the central nervous system. *Mech. Dev.* 138 (Pt 1), 26–36.

Vanlandewijck, M., He, L., Mae, M.A., Andrae, J., Ando, K., Del Gaudio, F., Nahar, K., Lebouvier, T., Lavina, B., Gouveia, L., et al. (2018). A molecular atlas of cell types and zonation in the brain vasculature. *Nature* 554, 475–480.

Vasudevan, A., Long, J.E., Crandall, J.E., Rubenstein, J.L., and Bhide, P.G. (2008). Compartment-specific transcription factors orchestrate angiogenesis gradients in the embryonic brain. *Nat. Neurosci.* 11, 429–439.

Walker, L.C., Parker, C.A., Lipinski, W.J., Callahan, M.J., Carroll, R.T., Gandy, S.E., Smith, J.D., Jucker, M., and Bisgaier, C.L. (1997). Cerebral lipid deposition in aged apolipoprotein-E-deficient mice. *Am. J. Pathol.* 151, 1371–1377.

Wang, L., Zhang, X., Pang, N., Xiao, L., Li, Y., Chen, N., Ren, M., Deng, X., and Wu, J. (2015). Glycation of vitronectin inhibits VEGF-induced angiogenesis by uncoupling VEGF receptor-2-alphavbeta3 integrin cross-talk. *Cell Death Dis.* 6, e1796.

Wang, J., Niu, N., Xu, S., and Jin, Z.G. (2019). A simple protocol for isolating mouse lung endothelial cells. *Sci. Rep.* 9, 1458.

Winkler, E.A., Bell, R.D., and Zlokovic, B.V. (2010). Pericyte-specific expression of PDGF beta receptor in mouse models with normal and deficient PDGF beta receptor signaling. *Mol. Neurodegener.* 5, 32.

Wu, H., Kirita, Y., Donnelly, E.L., and Humphreys, B.D. (2019). Advantages of single-nucleus over single-cell RNA sequencing of adult kidney: rare cell types and novel cell states revealed in fibrosis. *J. Am. Soc. Nephrol.* 30, 23–32.

Yeh, H.J., He, Y.Y., Xu, J., Hsu, C.Y., and Deuel, T.F. (1998). Upregulation of pleiotrophin gene expression in developing microvasculature, macrophages, and astrocytes after acute ischemic brain injury. *J. Neurosci.* 18, 3699–3707.

Yuzwa, S.A., Yang, G., Borrett, M.J., Clarke, G., Cancino, G.I., Zahr, S.K., Zandstra, P.W., Kaplan, D.R., and Miller, F.D. (2016). Proneurogenic ligands defined by modeling developing cortex growth factor communication networks. *Neuron* 91, 988–1004.

Zeisel, A., Hochgerner, H., Lonnerberg, P., Johnsson, A., Memic, F., van der Zwan, J., Haring, M., Braun, E., Borm, L.E., La Manno, G., et al. (2018). Molecular architecture of the mouse nervous system. *Cell* 174, 999–1014.e22.

Zhan, Y., Paolicelli, R.C., Sforazzini, F., Weinhard, L., Bolasco, G., Pagani, F., Vyssotski, A.L., Bifone, A., Gozzi, A., Ragozzino, D., et al. (2014). Deficient neuron-microglia signaling results in impaired functional brain connectivity and social behavior. *Nat. Neurosci.* 17, 400–406.

Zhang, Y., Chen, K., Sloan, S.A., Bennett, M.L., Scholze, A.R., O'Keeffe, S., Phatnani, H.P., Guarneri, P., Caneda, C., Ruderisch, N., et al. (2014). An RNA-sequencing transcriptome and splicing database of glia, neurons, and vascular cells of the cerebral cortex. *J. Neurosci.* 34, 11929–11947.

Zhang, Y., Sloan, S.A., Clarke, L.E., Caneda, C., Plaza, C.A., Blumenthal, P.D., Vogel, H., Steinberg, G.K., Edwards, M.S., Li, G., et al. (2016). Purification and characterization of progenitor and mature human astrocytes reveals transcriptional and functional differences with mouse. *Neuron* 89, 37–53.

Zhou, J.X., Taramelli, R., Pedrini, E., Knijnenburg, T., and Huang, S. (2017). Extracting intercellular signaling network of cancer tissues using ligand-receptor expression patterns from whole-tumor and single-cell transcriptomes. *Sci. Rep.* 7, 8815.

Supplemental Information

**Systematic Identification of Cell-Cell
Communication Networks in the Developing Brain**

**Bilal N. Sheikh, Olga Bondareva, Sukanya Guhathakurta, Tsz Hong Tsang, Katarzyna
Sikora, Nadim Aizarani, Sagar, Herbert Holz, Dominic Grün, Lutz Hein, and Asifa Akhtar**

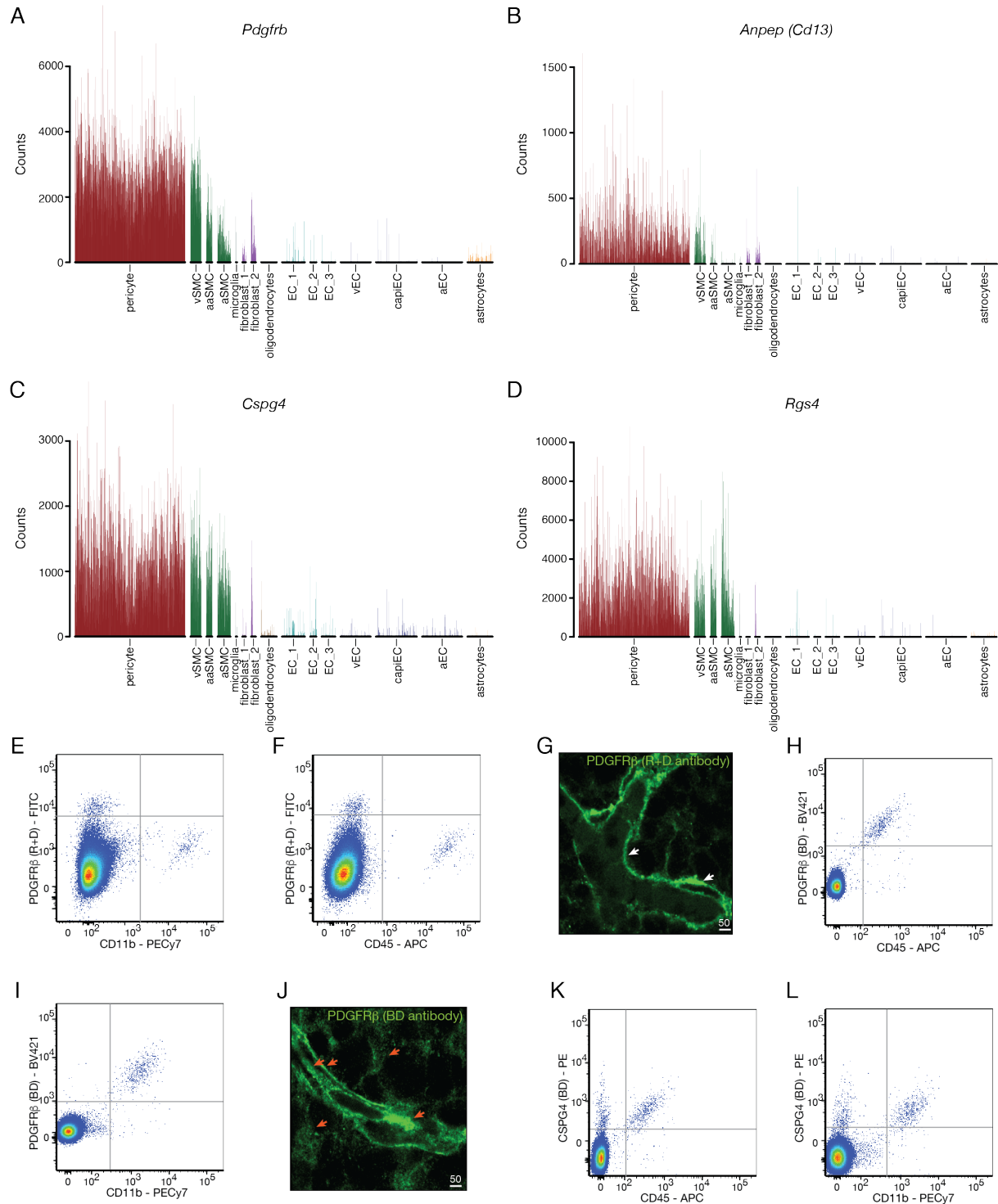


Figure S1

Screening for potential mural cell markers and antibodies.

Related to Figure 1

(A-D) Expression of potential mural cell markers in the published scRNA-seq database by the Betscholtz laboratory (Vanlandewijck et al., 2018). **(A)** *Pdgfrb* showed consistently high expression in all pericytes and smooth muscle cells. PDGFR β is expressed on the cell surface making it ideal for downstream use. **(B)** *Anpep (Cd13)* showed weak expression that was undetectable in some pericytes. While this may be due to the low sensitivity of scRNA-seq, it also suggests that CD13 expression may be heterogeneous within the mural cell population resulting in some pericytes and

smooth muscle cells remaining undetected. **(C)** *Cspg4* displayed strong expression in pericytes and smooth muscle cells and thus was shortlisted for downstream testing. **(D)** While *Rgs4* showed strong expression in pericytes and smooth muscle cells, it is an intracellular marker and thus not conducive to FACS. **(E)** Flow cytometry plot comparing the expression of PDGFR β (R+D antibody) and the microglia-specific marker CD11b. PDGFR β (R+D) antibody did not show any cross reactivity with CD11b. **(F)** Flow cytometry plot showing no overlap in staining with the PDGFR β (R+D) antibody and the microglia and hematopoietic marker CD45. **(G)** Immunofluorescence staining using the PDGFR β (R+D) antibody showing clear peri-vascular staining (white arrows) in the E14.5 brain cortex. Also see Figure 1C. **(H-I)** Flow cytometry plot showing cross-reactivity between the Becton Dickinson (BD) PDGFR β antibody and microglial markers **(H)** CD45 and **(I)** CD11b. **(J)** Immunofluorescence staining using the PDGFR β (BD) antibody showing unexpected intracellular staining in vascular cells as well as widespread background signal outside of the vasculature (marked by red arrows). **(K-L)** Flow cytometry plot showing cross-reactivity between the Becton Dickinson (BD) CSPG4 antibody and microglial markers **(K)** CD45 and **(L)** CD11b.

Based on these analyses, the BD PDGFR β and CSPG4 antibodies were not used and all experiments utilised the PDGFR β antibody from R+D.

N = 3 to 10 replicates per experiment in E-L.

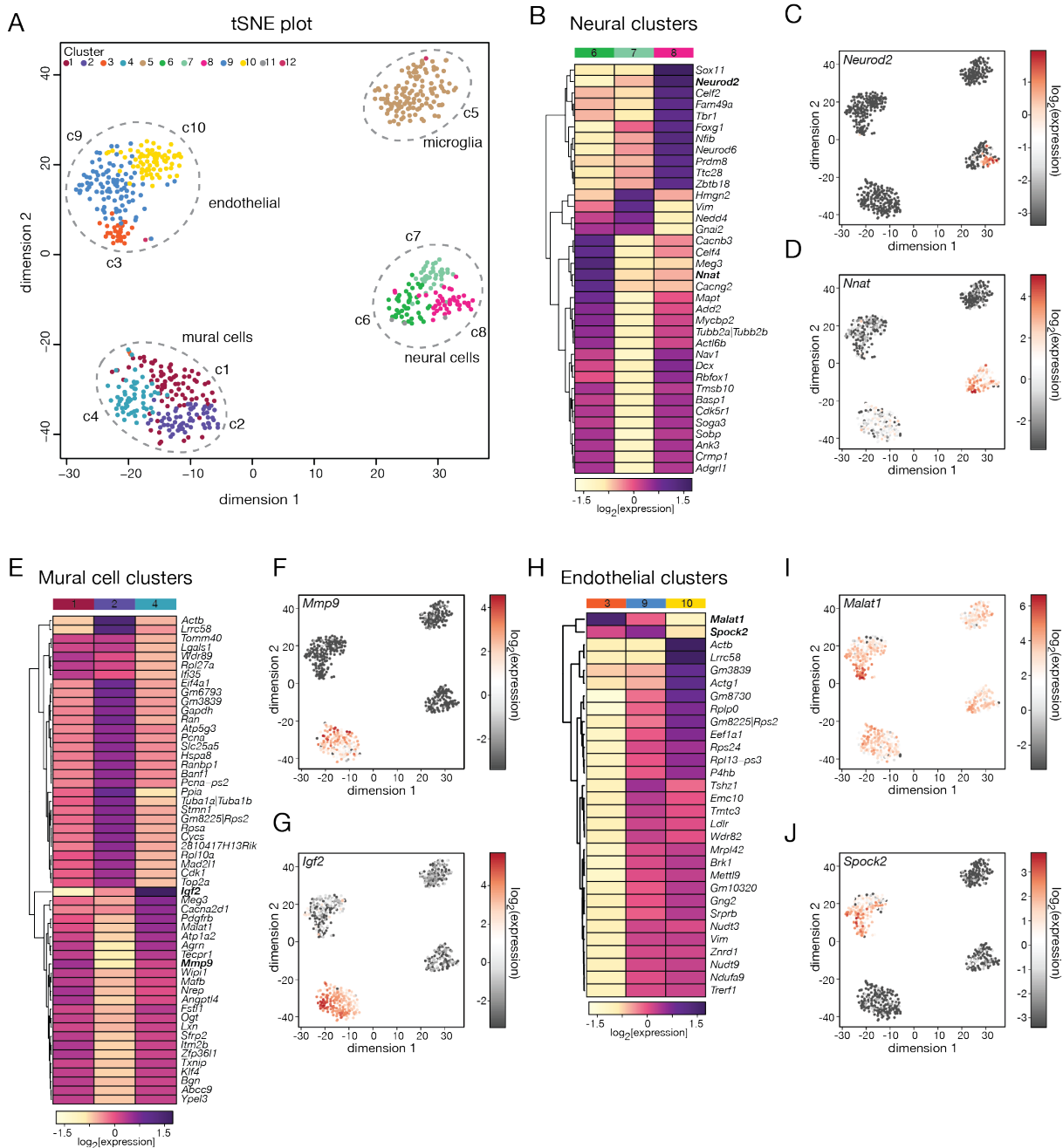


Figure S2

Comparison between subpopulations of neural cells, mural cells and endothelial cells.

Related to Figures 1 and 2

(A) An unbiased t-distributed stochastic neighbour embedding (tSNE) plot of all sorted cells, regardless of the cell surface marker used for their isolation, depicting 12 total clusters encompassing the four major cell populations: neural cells (clusters 6 to 8), mural cells (clusters 1, 2 and 4) endothelial cells (clusters 3, 9 and 10) and microglia (cluster 5). While each of the neural, mural and endothelial populations could be split into 3 three sub-clusters, only one cluster for microglia was evident. **(B)** Heatmap depicting differential gene expression between the three main sub-populations of the neural population. The $\log_2(\text{normalised counts})$ value is provided for the top differentially expressed genes that display an enrichment score of more than 1. **(C)** tSNE plot showing *Neurod2* mRNA enrichment in differentiating neurons (cluster 8) compared to the stem / progenitor stem cell population (cluster 6). **(D)** tSNE plot showing enrichment of *Nnat* in cluster 6. **(E)** Heatmap depicting differential gene expression between the three sub-populations of mural cells isolated based on

PDGFR β expression. The $\log_2(\text{normalised counts})$ value is provided for the top differentially expressed genes that display an absolute enrichment score of more than 0.6. **(F)** tSNE plot displaying expression of *Mmp9*, which is enriched in clusters 1 and 4, while lowly expressed in cluster 2. **(G)** tSNE plot of *Igf2* expression. *Igf2* shows strongest expression in cluster 4 and is significantly lower in clusters 1 and 2. **(H)** Heatmap depicting differential gene expression between the sub-populations of endothelial cells isolated based on PECAM1 and CD102 expression. The $\log_2(\text{normalised counts})$ value is provided for the top differentially expressed genes that display an absolute enrichment score of more than 1. **(I)** tSNE plot showing *Malat1* expression. While *Malat1* is widely expressed, it shows the highest gene expression in cluster 3 of endothelial cells. **(J)** tSNE plot showing gradient of *Spock2* gene expression.

The enrichment score was calculated by determining the expression of a particular gene in the given cell cluster relative to the mean expression of that same gene across all clusters.

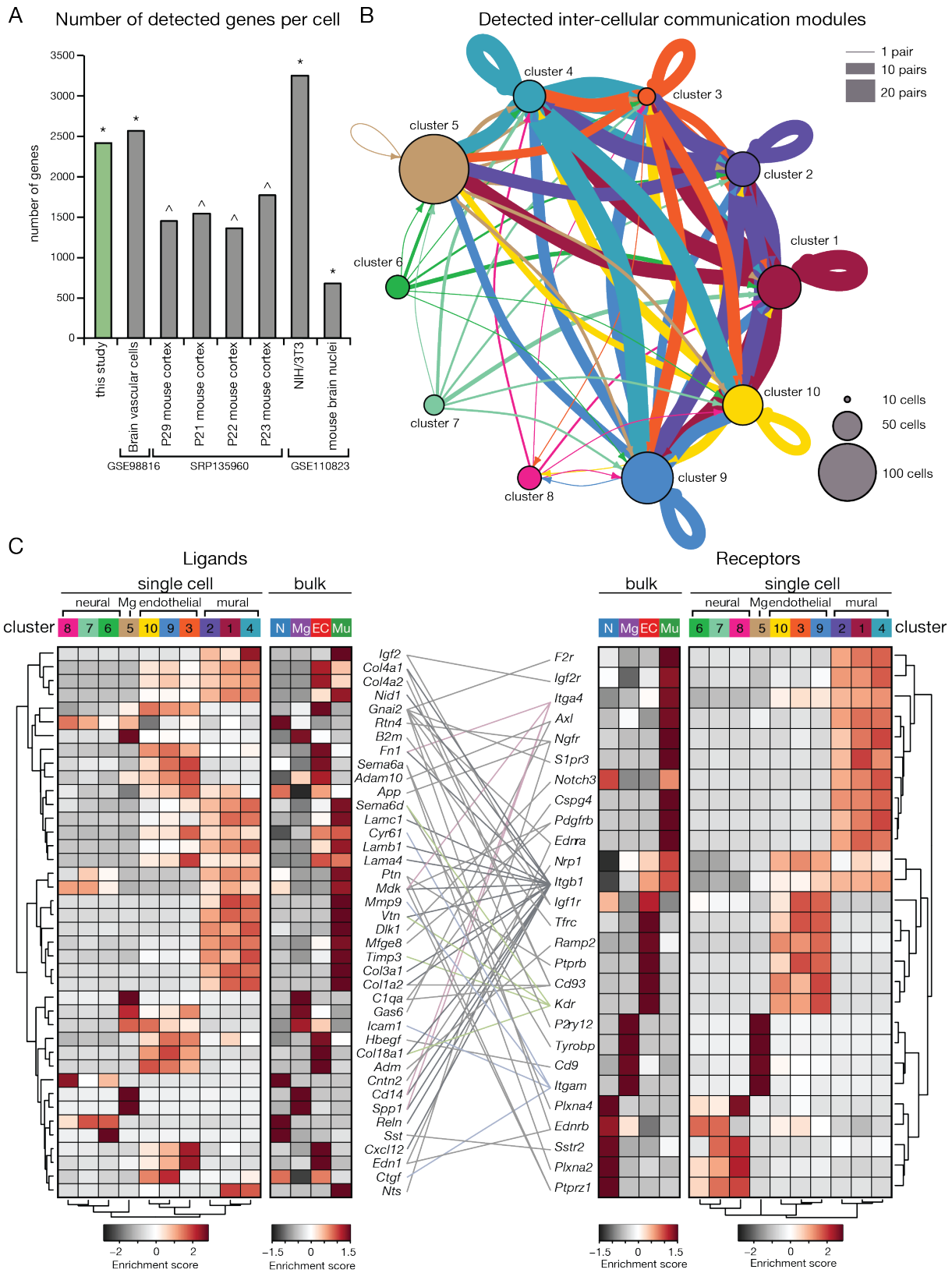


Figure S3

Cell-cell communication networks between neural, mural, endothelial and microglial cell clusters detected in the scRNA-seq dataset.

Related to Figures 3 and 4

(A) Comparison of the number of unique genes detected in scRNA-seq datasets. The GSE98816 dataset is associated with (Vanlandewijck et al., 2018), the SRP135960 dataset with (Zeisel et al.,

2018) and the GSE110823 dataset with (Rosenberg et al., 2018). * indicate the mean number of genes detected per cell, while ^ represents the median number of genes detected per cell. Note that at greater, saturated sequencing depth (>500,000 reads per cell), Rosenberg et al. (2018) report a mean of 4497 detected genes per NIH/3T3 cell and 2055 genes per brain nucleus. **(B)** Inter-cellular interaction network of ligands and receptors between the 10 major clusters identified from the scRNA-seq data. A total of 80 ligands and 61 receptors were expressed in at least one cell cluster without taking into consideration the existence of the complete pair. 61 pairs encompassing 40 ligands and 27 receptors were detected in the whole database. The ligand – receptor interactions were based on the dataset curated by (Ramilowski et al., 2015). The thickness of lines connecting the respective clusters indicates the number of ligand – receptor interactions between the clusters. The size of the cluster circle represents the number of cells identified in the particular cluster. **(C)** Heatmaps showing the enrichment of ligands and receptors in each cluster of the scRNA-seq data as well as in bulk EMBRACE-isolated populations. Lines connecting ligand and receptor pairs depict the interaction between them.

The enrichment score was calculated for scRNA-seq data by determining the expression of a particular gene in the given cell cluster relative to the mean expression of that same gene across all clusters. For bulk RNA-seq analyses, the enrichment score was quantified by determining the expression of a particular gene in a specific cell type relative to the mean expression of that same gene across all 4 EMBRACE-isolated cell populations.

EC – endothelial cells, Mg – microglia, Mu – mural cells, N – neural cells

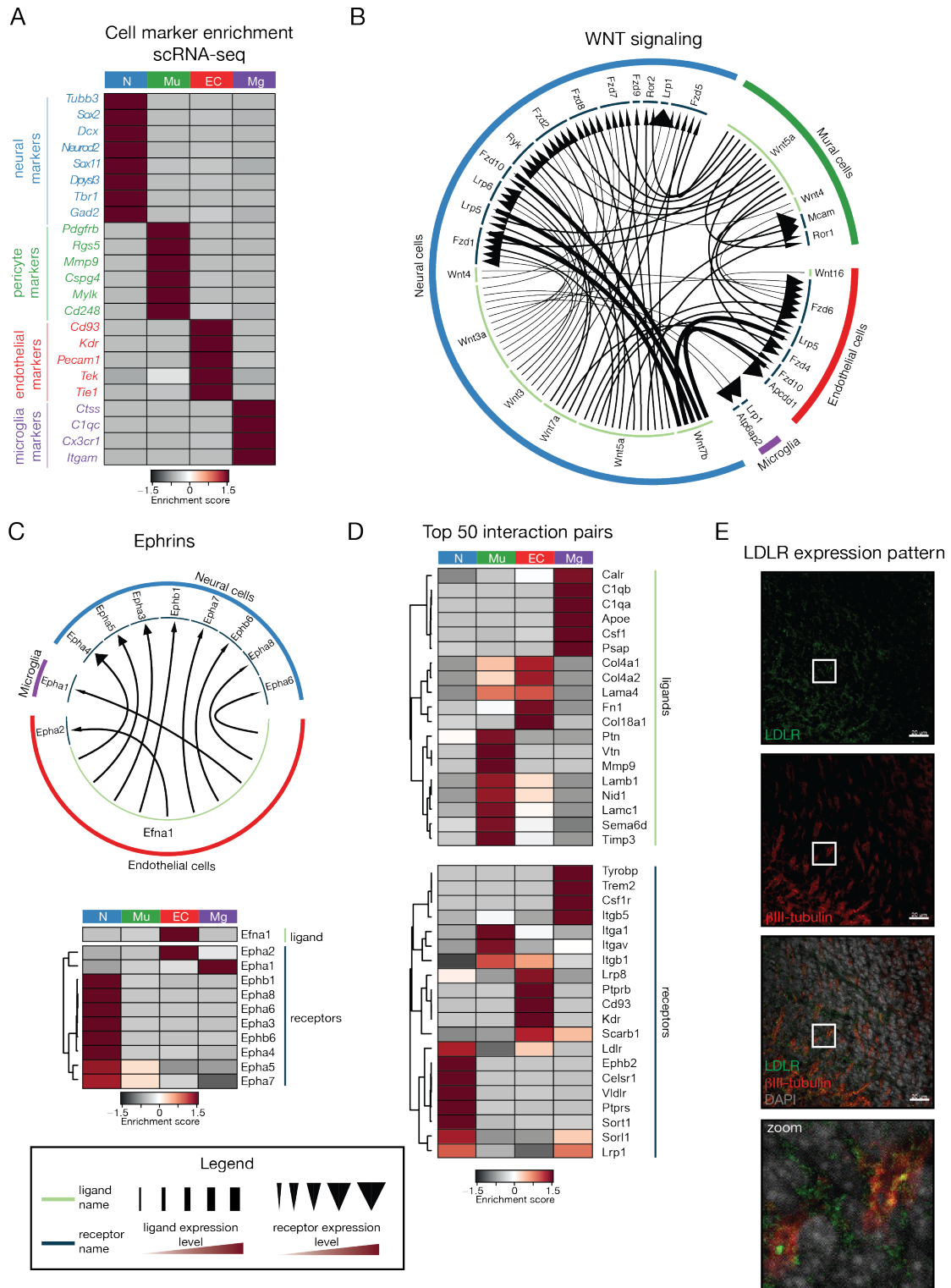


Figure S4

Key communication networks in neural, mural, endothelial and microglial cell populations

Related to Figures 4 and 5

(A) Enrichment of cell type markers in the scRNA-seq dataset for each cell type. **(B)** Interaction ligand-receptor map for WNT signaling based on transcriptomic analyses on bulk sorted populations. Note the high number of interactions involving neural cells. **(C)** Interaction map for Ephrin A1 (*Efna1*), which is highly enriched in endothelial cells, and its receptors, which are primarily expressed in neural cells. The heatmap displays enrichment in gene expression of Ephrin A1 and its receptors in the different

cell populations based on the enrichment score. **(D)** Heatmap based on the interaction map provided in Figure 4F. The heatmap displays gene expression of the 50 highest scoring ligand-receptor pairs bioinformatically mapped in the developing brain. The enrichment of each ligand and receptor is shown based on the enrichment score in neural, mural, endothelial and microglial cells. **(E)** Immunofluorescence images showing widespread expression of LDLR, especially in β III-tubulin positive neurons in the E14.5 brain. Scale bars indicate 20 μ m.

The enrichment score was calculated by determining the expression of a particular gene in a specific cell type relative to the mean expression of that same gene across all 4 EMBRACE-isolated cell populations.

EC – endothelial cells, Mg – microglia, Mu – mural cells, N – neural cells

Table S1*Related to Figure 1*

Comparison of methods used for the dissociation of E14.5 brains. The scale spans “-” not detected, to “++++” present at highest levels. “Clumpiness” and “Digestion” were determined by the fraction of cells failing to pass through a 100 µm filter after digestion. Ease of digestion was determined by the amount of manual pipetting required to dissociate the tissue until no obvious tissue clumps were visible.

	No enzyme	Collagenase Dispase	Pancreatin Trypsin	Liberase only	Liberase + Dnase I
Ease of dissociation	++++	++	++++	+++	+++
Clumpiness	-	++	+++	++	-
Digestion	++++	++	+++	+++	++++
Survival (%)*	17 ± 1.7	39.5 ± 2.2	55.9 ± 1.4	46.6 ± 2.6	67.8 ± 0.7
Median Fluorescence Intensity (MFI, PECAM1)	464	308	94	421	not assessed

* proportion of live FACS events as a proportion of total sorted events

Table S2*Related to Figures 1 to 5*

List of antibodies used and their specificity. Antibodies shown in red were found to be specific and used in this study. Concentrations provided are for use in immunofluorescence. For Western Blot analysis, antibodies were used at 1:1000. For FACS, the secondary Alexa488-conjugated anti-goat IgG (A11055 ThermoFisher, 1:400) was used to detect the primary PDGFR β (R+D systems) antibody.

Antibody	Code and Provider	Concentration	Specific?
APOE	Polyclonal 178479 Merck	1:250	Yes
β -III tubulin	clone 5G8 Promega	1:1000	Yes
CD11b	clone M1/70 BD	1:300	Yes
CD13	clone EM15 eBioscience	1:100	Yes, but low signal
CD41	clone MWReg30 BD	1:200	Yes
CD45	clone 30-F11 BD	1:300	Yes
IBA1	EPR16588 (ab178846) Abcam	1:1000	Yes
ICAM2 (CD102)	clone 3C4(mIC2/4) BD	1:250	Yes
KDR (FLK1, VEGFR2)	clone D-8 (sc-393163) Santa Cruz	1:200	Yes
ITGB1	Polyclonal sc-8978 Santa Cruz	1:200	Yes
LAMA4	CL3183 (ab242198) Abcam	1:200	Yes
LDLR	EPY1553Y (ab52818) Abcam	1:250	Yes
LRP1	EPR3724 (ab92544) Abcam	1:250	Yes
NG2 (CSPG4)	clone 9.2.27 BD	1:100	No
NG2 (CSPG4)	Polyclonal AB5320 Millipore	1:100	No
PDGFR β (CD140b)	clone 28D4 BD	1:200	No
PDGFR β (CD140b)	Polyclonal AF1042 R+D systems	1:200	Yes
PECAM1 (CD31)	clone 390 eBioscience	1:250	Yes
PECAM1 (CD31)	Polyclonal ab28364 Abcam	1:100	Yes
VTN	EP873Y (ab45139) Abcam	1:200	Yes

Table S3

Related to Figure 2

List of genes most strongly enriched in neural clusters of the scRNA-seq dataset.

Gene	base Mean	Base MeanA	Base MeanB	fold- enrichment	log2 [enrichment]	p value	FDR
Dpysl3	1.19	0.13	2.24	17.68	4.14	6.70E-130	1.90E-126
Rtn1	1.06	0.13	2.00	15.64	3.97	6.18E-112	1.50E-108
Tubb3	0.91	0.11	1.71	15.46	3.95	4.31E-95	8.63E-92
Sox11	4.10	0.54	7.65	14.16	3.82	0.00E+00	0.00E+00
Elavl3	0.78	0.11	1.45	12.94	3.69	7.76E-76	1.15E-72
Stmn2	0.83	0.12	1.54	12.83	3.68	9.97E-80	1.79E-76
Dcx	0.67	0.10	1.23	11.68	3.55	6.39E-62	7.76E-59
Cd24a	1.00	0.16	1.83	11.25	3.49	1.52E-90	2.88E-87
Nsg2	0.64	0.11	1.17	10.86	3.44	2.16E-57	2.37E-54
Bcl11b	0.59	0.11	1.07	9.55	3.26	2.85E-49	2.55E-46
Nnat	3.53	0.68	6.38	9.38	3.23	0.00E+00	0.00E+00
Foxg1	0.55	0.11	0.99	9.27	3.21	1.66E-45	1.31E-42
Elavl4	0.58	0.12	1.05	9.14	3.19	9.49E-48	7.69E-45
Mapt	0.60	0.12	1.09	9.05	3.18	9.61E-49	8.39E-46
Map1b	2.02	0.41	3.62	8.86	3.15	5.05E-154	2.46E-150
Gpm6a	0.54	0.12	0.97	8.39	3.07	8.14E-43	5.90E-40
Map2	0.61	0.13	1.10	8.37	3.07	7.11E-48	5.90E-45
Gap43	0.50	0.11	0.90	8.29	3.05	4.32E-39	2.59E-36
Sbk1	0.51	0.11	0.90	8.22	3.04	1.25E-39	7.86E-37
Neurod6	0.48	0.11	0.85	7.95	2.99	1.03E-35	5.33E-33
Igfbp1	0.46	0.10	0.81	7.85	2.97	7.63E-35	3.71E-32
Lhx2	0.47	0.11	0.83	7.67	2.94	3.51E-35	1.79E-32
Meis2	0.46	0.11	0.81	7.46	2.90	1.01E-32	4.28E-30
Pou3f3	0.46	0.11	0.80	7.45	2.90	1.01E-32	4.28E-30
Sox2	0.49	0.12	0.86	7.38	2.88	5.39E-35	2.66E-32
Kif5c	0.44	0.11	0.78	7.30	2.87	1.67E-31	6.67E-29
Ina	0.45	0.11	0.79	7.23	2.85	1.01E-32	4.28E-30
Nfib	1.75	0.43	3.06	7.05	2.82	6.69E-117	1.75E-113
Elavl2	0.43	0.11	0.76	6.90	2.79	3.89E-30	1.52E-27
Miat	0.42	0.11	0.74	6.87	2.78	1.93E-29	7.11E-27
Dclk1	0.42	0.11	0.73	6.85	2.78	2.03E-28	7.26E-26
Trim2	0.43	0.11	0.76	6.84	2.77	8.27E-30	3.09E-27
Tubb2a Tubb2b	2.52	0.65	4.38	6.73	2.75	3.10E-147	1.32E-143
37865	0.40	0.10	0.70	6.73	2.75	3.22E-27	1.10E-24
Pak3	0.43	0.11	0.74	6.52	2.70	3.66E-28	1.30E-25
Bcl11a	0.54	0.14	0.93	6.46	2.69	1.63E-34	7.81E-32
Runx1t1	0.42	0.11	0.73	6.34	2.67	3.64E-27	1.22E-24
Neurod2	0.38	0.10	0.65	6.29	2.65	5.11E-25	1.58E-22
Celf2	1.19	0.33	2.05	6.22	2.64	4.27E-73	6.05E-70
Celf4	0.39	0.11	0.68	6.21	2.64	4.23E-25	1.32E-22
Ank3	0.41	0.11	0.70	6.19	2.63	5.56E-26	1.77E-23
Nfix	0.48	0.13	0.82	6.12	2.61	4.36E-30	1.67E-27
Nsg1	0.42	0.12	0.72	6.08	2.60	4.48E-26	1.44E-23
Gria2	0.37	0.10	0.63	6.00	2.59	9.53E-23	2.64E-20
Cntn2	0.40	0.12	0.69	5.89	2.56	6.65E-25	2.04E-22
Cdk5r1	0.53	0.15	0.91	5.89	2.56	4.79E-32	1.94E-29
Dlx1	0.36	0.11	0.61	5.81	2.54	8.88E-22	2.34E-19
Pbx1	0.88	0.26	1.49	5.74	2.52	1.06E-50	1.06E-47
Crmp1	0.57	0.17	0.97	5.67	2.50	7.08E-33	3.13E-30
Stmn1	2.63	0.80	4.47	5.61	2.49	4.57E-130	1.41E-126
Basp1	2.11	0.64	3.58	5.58	2.48	1.24E-111	2.81E-108
Tagln3	0.47	0.15	0.79	5.38	2.43	3.24E-26	1.05E-23
Soga3	0.37	0.12	0.63	5.32	2.41	7.89E-21	1.99E-18
Kif21a	0.37	0.12	0.62	5.23	2.39	2.29E-20	5.49E-18
Fez1	0.34	0.11	0.57	5.21	2.38	4.40E-19	9.72E-17
St8sia2	0.35	0.11	0.59	5.20	2.38	2.74E-19	6.22E-17
Epha4	0.39	0.13	0.65	4.92	2.30	1.09E-20	2.68E-18
6330403K07Rik	0.35	0.12	0.58	4.89	2.29	4.30E-18	9.04E-16
Insm1	0.30	0.10	0.50	4.88	2.29	5.62E-16	9.75E-14
Zfp462	0.46	0.16	0.76	4.87	2.28	7.83E-24	2.28E-21
Pfn2	0.44	0.15	0.74	4.82	2.27	1.60E-22	4.33E-20
Rnd2	0.32	0.11	0.53	4.82	2.27	4.73E-17	8.99E-15
Milt11	0.38	0.13	0.62	4.77	2.25	6.73E-19	1.47E-16
Neurog2	0.30	0.10	0.50	4.74	2.24	2.70E-15	4.38E-13
Kif1a	0.30	0.11	0.49	4.59	2.20	1.25E-14	1.88E-12
Gng3	0.31	0.11	0.51	4.59	2.20	4.76E-15	7.43E-13
Mpped2	0.35	0.13	0.57	4.57	2.19	2.17E-17	4.22E-15
Pantr1	0.31	0.11	0.51	4.55	2.19	1.74E-15	2.88E-13
Gm3764	0.30	0.11	0.49	4.55	2.19	1.25E-14	1.88E-12
Tmeff1	0.32	0.12	0.52	4.54	2.18	6.64E-16	1.14E-13
Dpysl5	0.29	0.11	0.47	4.49	2.17	2.03E-14	2.98E-12
Tbr1	0.28	0.10	0.46	4.48	2.16	8.96E-14	1.24E-11
Ppp2r2b	0.28	0.10	0.46	4.45	2.15	8.96E-14	1.24E-11
Neurod1	0.27	0.10	0.45	4.38	2.13	1.46E-13	1.97E-11

<i>Plxna2</i>	0.37	0.14	0.60	4.34	2.12	<i>1.47E-17</i>	2.92E-15
<i>Cnih2</i>	0.30	0.11	0.49	4.32	2.11	<i>3.49E-14</i>	4.99E-12
<i>Bex2</i>	0.28	0.11	0.45	4.31	2.11	<i>1.48E-13</i>	2.00E-11
<i>Pou3f2</i>	0.30	0.11	0.48	4.31	2.11	<i>3.46E-14</i>	4.97E-12
<i>Zbtb18</i>	0.43	0.17	0.70	4.22	2.08	<i>3.14E-19</i>	7.03E-17
<i>Myt1l</i>	0.26	0.10	0.42	4.22	2.08	<i>2.77E-12</i>	3.42E-10
<i>Mir124-2hg</i>	0.27	0.10	0.43	4.20	2.07	<i>1.70E-12</i>	2.14E-10
<i>Camta1</i>	0.31	0.12	0.50	4.20	2.07	<i>1.32E-14</i>	1.97E-12
<i>Sox5</i>	0.32	0.12	0.51	4.14	2.05	<i>3.46E-14</i>	4.97E-12
<i>Mex3a</i>	0.58	0.23	0.93	4.04	2.02	<i>1.15E-23</i>	3.31E-21
<i>Ndn</i>	0.50	0.20	0.80	4.04	2.01	<i>9.95E-21</i>	2.47E-18
<i>Setbp1</i>	0.38	0.15	0.61	4.02	2.01	<i>2.63E-16</i>	4.66E-14
<i>Ttc3</i>	1.47	0.59	2.36	4.02	2.01	<i>4.41E-58</i>	5.01E-55
<i>Stmn3</i>	0.27	0.11	0.43	4.02	2.01	<i>4.37E-12</i>	5.29E-10
<i>Ptprz1</i>	0.29	0.12	0.46	4.00	2.00	<i>2.52E-12</i>	3.14E-10
<i>Srgap3</i>	0.27	0.11	0.43	3.99	2.00	<i>1.76E-11</i>	2.06E-09
<i>Sox4</i>	1.52	0.61	2.43	3.98	1.99	<i>3.68E-59</i>	4.32E-56
<i>Cxadr</i>	0.25	0.10	0.41	3.96	1.99	<i>7.55E-11</i>	8.10E-09
<i>Hdgfrp3</i>	0.33	0.13	0.52	3.92	1.97	<i>1.33E-13</i>	1.80E-11
<i>Stmn4</i>	0.26	0.10	0.41	3.91	1.97	<i>4.64E-11</i>	5.13E-09
<i>Fezf2</i>	0.26	0.11	0.42	3.91	1.97	<i>2.86E-11</i>	3.25E-09
<i>Rufy3</i>	0.37	0.15	0.58	3.90	1.96	<i>4.33E-15</i>	6.86E-13
<i>Ptbp2</i>	0.37	0.15	0.59	3.89	1.96	<i>1.71E-15</i>	2.85E-13
<i>Epha5</i>	0.34	0.14	0.55	3.88	1.95	<i>1.92E-14</i>	2.83E-12
<i>2610203C20Rik</i>	0.26	0.11	0.41	3.85	1.94	<i>7.20E-11</i>	7.80E-09
<i>Gnao1</i>	0.32	0.13	0.51	3.83	1.94	<i>3.34E-13</i>	4.41E-11

Table S4

Related to Figure 2

List of genes most strongly enriched in mural cell clusters of the scRNA-seq dataset.

Gene	Base Mean	Base MeanA	Base MeanB	fold-enrichment	log2 [enrichment]	p value	FDR
<i>Rgs5</i>	7.38	0.28	14.49	52.50	5.71	0.00E+00	0.00E+00
<i>Mmp9</i>	2.34	0.14	4.54	33.12	5.05	0.00E+00	0.00E+00
<i>Vtn</i>	2.02	0.15	3.90	26.66	4.74	0.00E+00	0.00E+00
<i>Igf2</i>	7.50	0.65	14.34	21.97	4.46	0.00E+00	0.00E+00
<i>Atp1a2</i>	1.61	0.15	3.07	20.34	4.35	2.63E-222	1.49E-218
<i>Abcc9</i>	1.54	0.15	2.93	19.04	4.25	1.27E-207	6.16E-204
<i>Cd248</i>	0.85	0.11	1.58	13.84	3.79	2.42E-103	6.35E-100
<i>Cald1</i>	2.30	0.32	4.28	13.38	3.74	6.53E-255	4.45E-251
<i>Kcnj8</i>	0.77	0.11	1.43	12.87	3.69	1.50E-91	2.83E-88
<i>Pcdh18</i>	1.06	0.15	1.97	12.86	3.69	1.26E-125	4.28E-122
<i>Myl9</i>	0.88	0.13	1.64	12.33	3.62	7.53E-103	1.83E-99
<i>Cspg4</i>	0.75	0.11	1.38	12.29	3.62	1.74E-86	2.58E-83
<i>Pdgfrb</i>	0.68	0.11	1.25	11.75	3.55	1.89E-77	2.39E-74
<i>Mylk</i>	0.82	0.14	1.49	10.29	3.36	5.20E-87	8.05E-84
<i>Heyl</i>	0.58	0.11	1.05	9.67	3.27	4.27E-60	3.54E-57
<i>Gjc1</i>	0.96	0.19	1.74	9.29	3.22	4.00E-97	8.01E-94
<i>Ednra</i>	0.56	0.11	1.01	9.05	3.18	1.31E-56	9.90E-54
<i>Dlk1</i>	0.74	0.15	1.32	9.04	3.18	6.24E-74	6.85E-71
<i>Col3a1</i>	0.56	0.11	1.00	8.86	3.15	3.04E-55	2.25E-52
<i>Rgs4</i>	0.65	0.13	1.17	8.79	3.14	3.81E-64	3.51E-61
<i>Ndufa4l2</i>	0.49	0.11	0.86	7.97	2.99	3.31E-45	1.94E-42
<i>Notch3</i>	0.54	0.12	0.97	7.90	2.98	9.65E-51	6.57E-48
<i>F2r</i>	0.87	0.21	1.53	7.32	2.87	2.35E-75	2.76E-72
<i>Fstl1</i>	1.46	0.35	2.57	7.29	2.87	3.29E-125	1.02E-121
<i>Col1a2</i>	0.43	0.11	0.76	7.08	2.82	4.32E-38	2.02E-35
<i>Gucy1b3</i>	0.45	0.11	0.79	7.05	2.82	1.54E-39	7.59E-37
<i>Gucy1a3</i>	0.45	0.11	0.79	6.95	2.80	1.08E-38	5.11E-36
<i>Atp1b2</i>	0.51	0.14	0.89	6.54	2.71	4.68E-42	2.53E-39
40787	1.33	0.36	2.30	6.46	2.69	1.11E-105	3.16E-102
<i>Ngfr</i>	0.43	0.12	0.73	6.25	2.64	5.67E-34	2.33E-31
<i>S1pr3</i>	0.38	0.10	0.65	6.22	2.64	5.22E-30	1.76E-27
<i>Zic1</i>	0.91	0.26	1.57	6.12	2.61	4.22E-70	4.11E-67
<i>Meg3</i>	1.97	0.57	3.37	5.95	2.57	1.55E-141	5.86E-138
<i>Sdc2</i>	0.38	0.11	0.65	5.77	2.53	2.08E-28	6.80E-26
<i>Mfge8</i>	0.66	0.20	1.12	5.63	2.49	1.32E-47	8.50E-45
<i>Farp1</i>	0.45	0.14	0.76	5.54	2.47	1.38E-32	5.15E-30
<i>Axl</i>	0.48	0.15	0.81	5.36	2.42	1.52E-33	6.10E-31
<i>Gm13889</i>	0.46	0.15	0.78	5.32	2.41	3.73E-32	1.35E-29
<i>Gper1</i>	0.33	0.11	0.54	4.98	2.31	6.98E-22	1.77E-19
<i>Uaca</i>	0.51	0.17	0.84	4.93	2.30	5.82E-33	2.20E-30
<i>S100a11</i>	0.57	0.19	0.95	4.92	2.30	4.23E-37	1.89E-34
<i>Tbx2a2r</i>	0.35	0.12	0.57	4.87	2.28	1.75E-22	4.59E-20
<i>Mmp11</i>	0.30	0.10	0.50	4.85	2.28	3.91E-20	9.30E-18
<i>Pde8b</i>	0.32	0.11	0.54	4.84	2.27	5.11E-21	1.27E-18
<i>Lhfp</i>	0.36	0.12	0.59	4.81	2.27	6.04E-23	1.60E-20
<i>Foxd1</i>	0.30	0.10	0.49	4.72	2.24	2.82E-19	6.27E-17
38231	0.45	0.16	0.73	4.67	2.22	1.11E-27	3.48E-25
<i>Pde5a</i>	0.37	0.13	0.60	4.54	2.18	1.18E-22	3.12E-20
<i>Tppp3</i>	0.36	0.13	0.58	4.48	2.16	5.71E-22	1.46E-19
<i>Hspa1a/Hspa1b</i>	0.89	0.33	1.45	4.42	2.14	1.01E-50	6.73E-48
<i>Bgn</i>	1.44	0.54	2.35	4.32	2.11	3.44E-79	4.51E-76
39326	1.39	0.52	2.26	4.31	2.11	6.70E-76	8.15E-73
<i>Akap12</i>	0.61	0.23	1.00	4.31	2.11	2.67E-34	1.11E-31
<i>Rian</i>	0.50	0.19	0.81	4.25	2.09	7.17E-28	2.30E-25
<i>Trpc3</i>	0.28	0.11	0.46	4.24	2.08	1.95E-16	3.71E-14
<i>Plce1</i>	0.29	0.11	0.47	4.22	2.08	4.05E-17	8.01E-15
<i>Mcam</i>	0.82	0.31	1.32	4.22	2.08	1.35E-44	7.64E-42
<i>Gnas</i>	0.85	0.33	1.38	4.20	2.07	1.40E-45	8.34E-43
<i>Phlda1</i>	0.75	0.29	1.20	4.18	2.06	5.02E-40	2.59E-37
<i>Gadd45b</i>	0.43	0.17	0.69	4.11	2.04	5.73E-23	1.54E-20
<i>Tbx2</i>	0.29	0.11	0.46	4.10	2.04	3.97E-16	7.30E-14
<i>Lamb1</i>	0.90	0.36	1.44	4.06	2.02	1.83E-46	1.16E-43
<i>Fos</i>	1.75	0.69	2.81	4.06	2.02	1.83E-88	2.96E-85
<i>Arhgap42</i>	0.31	0.13	0.50	3.99	2.00	3.38E-17	6.73E-15
<i>Arhgef17</i>	0.30	0.12	0.47	3.96	1.99	1.33E-15	2.40E-13
<i>Gprc5c</i>	0.25	0.10	0.40	3.96	1.98	1.10E-13	1.75E-11
<i>Nid1</i>	1.74	0.71	2.76	3.92	1.97	6.49E-84	9.21E-81
<i>Ifitm3</i>	0.35	0.14	0.56	3.87	1.95	3.05E-18	6.41E-16
<i>Ptn</i>	0.64	0.26	1.02	3.87	1.95	1.22E-31	4.32E-29
<i>Higd1b</i>	0.25	0.10	0.40	3.85	1.95	3.14E-13	4.82E-11
<i>Eva1b</i>	0.51	0.21	0.81	3.82	1.93	6.24E-25	1.82E-22
<i>Tns1</i>	0.42	0.17	0.66	3.80	1.93	1.89E-20	4.55E-18
<i>Epb41l1</i>	0.31	0.13	0.49	3.77	1.92	4.84E-16	8.87E-14
<i>Lgals1</i>	0.35	0.15	0.55	3.76	1.91	1.37E-17	2.82E-15

<i>Cdh11</i>	0.39	0.17	0.62	3.73	1.90	7.87E-19	1.70E-16
<i>Tnfrsf21</i>	0.48	0.20	0.76	3.72	1.90	2.12E-23	5.87E-21
<i>Igf2r</i>	0.51	0.22	0.80	3.66	1.87	5.83E-24	1.65E-21
<i>Ebf1</i>	0.79	0.34	1.24	3.65	1.87	3.94E-36	1.72E-33
<i>Gstk1</i>	0.25	0.11	0.40	3.63	1.86	6.71E-13	1.01E-10
<i>Afap1l2</i>	0.25	0.11	0.40	3.63	1.86	2.12E-12	3.03E-10
<i>Atp7a</i>	0.45	0.20	0.71	3.58	1.84	7.43E-21	1.83E-18
<i>Pdlim2</i>	0.26	0.11	0.40	3.58	1.84	4.38E-12	6.18E-10
<i>Spry4</i>	0.26	0.11	0.40	3.55	1.83	2.30E-12	3.27E-10
<i>Adap2</i>	0.33	0.15	0.52	3.53	1.82	2.38E-15	4.22E-13
<i>Sema6d</i>	1.00	0.44	1.56	3.53	1.82	2.05E-43	1.14E-40
<i>Dmd</i>	0.26	0.11	0.41	3.53	1.82	1.92E-12	2.77E-10
<i>Col5a1</i>	0.25	0.11	0.39	3.51	1.81	1.00E-11	1.36E-09
<i>Oaz2</i>	0.71	0.31	1.10	3.51	1.81	8.33E-31	2.92E-28
<i>Timp3</i>	0.45	0.20	0.70	3.49	1.80	1.63E-20	3.99E-18
<i>Sfrp2</i>	0.25	0.11	0.38	3.46	1.79	1.00E-11	1.36E-09
<i>Zfp703</i>	0.44	0.20	0.68	3.46	1.79	1.57E-19	3.56E-17
<i>Pid1</i>	0.35	0.16	0.54	3.45	1.79	2.50E-15	4.40E-13
<i>Hic1</i>	0.29	0.13	0.44	3.45	1.79	6.07E-13	9.22E-11
<i>Tlr12</i>	0.27	0.12	0.42	3.45	1.79	1.43E-12	2.09E-10
<i>Tbx18</i>	0.23	0.10	0.35	3.41	1.77	2.24E-10	2.66E-08
<i>Car4</i>	0.23	0.10	0.36	3.41	1.77	6.54E-11	8.15E-09
<i>Rasl12</i>	0.23	0.11	0.36	3.41	1.77	9.84E-11	1.19E-08
<i>Lamc3</i>	0.23	0.11	0.36	3.39	1.76	9.84E-11	1.19E-08
<i>Slc19a1</i>	0.24	0.11	0.37	3.34	1.74	7.09E-11	8.81E-09
<i>Myh9</i>	0.76	0.35	1.16	3.31	1.73	1.87E-30	6.48E-28

Table S5

Related to Figure 2

List of genes most strongly enriched in endothelial clusters of the scRNA-seq dataset.

Gene	Base Mean	Base MeanA	Base MeanB	fold-enrichment	log2 [enrichment]	p value	FDR
<i>Cldn5</i>	1.73	0.12	3.35	28.42	4.83	5.81E-260	9.88E-256
<i>Kdr</i>	1.73	0.13	3.32	25.30	4.66	6.89E-252	7.81E-248
<i>Cd93</i>	1.62	0.13	3.11	24.54	4.62	1.48E-234	1.26E-230
<i>Spock2</i>	1.45	0.16	2.74	17.58	4.14	1.13E-189	5.50E-186
<i>Flt1</i>	1.50	0.16	2.83	17.28	4.11	1.28E-196	7.26E-193
<i>Slc2a1</i>	1.52	0.19	2.84	15.07	3.91	2.55E-189	1.08E-185
<i>Vwa1</i>	0.84	0.12	1.57	12.92	3.69	3.23E-99	7.33E-96
<i>Slc7a5</i>	1.38	0.21	2.55	11.86	3.57	9.76E-157	3.32E-153
<i>Slc38a5</i>	0.67	0.11	1.24	11.15	3.48	5.20E-75	7.08E-72
<i>Ptprb</i>	0.71	0.12	1.29	10.78	3.43	5.98E-77	8.85E-74
<i>Egf17</i>	0.76	0.13	1.38	10.76	3.43	2.26E-82	4.05E-79
<i>Slc7a1</i>	1.87	0.32	3.42	10.63	3.41	2.80E-199	1.91E-195
<i>Tie1</i>	0.71	0.13	1.29	9.80	3.29	1.78E-74	2.25E-71
<i>Pecam1</i>	0.63	0.12	1.15	9.76	3.29	6.48E-66	7.12E-63
<i>Mfsd2a</i>	0.54	0.11	0.96	8.68	3.12	8.71E-53	6.89E-50
<i>Mmrn2</i>	0.55	0.12	0.98	8.49	3.09	5.38E-53	4.36E-50
<i>Slc38a3</i>	0.51	0.11	0.90	8.34	3.06	2.50E-48	1.70E-45
<i>Htra3</i>	0.51	0.11	0.91	7.95	2.99	1.18E-47	7.90E-45
<i>Cd34</i>	0.61	0.14	1.09	7.95	2.99	1.32E-56	1.25E-53
<i>Cdh5</i>	0.44	0.11	0.78	7.26	2.86	1.83E-39	1.01E-36
<i>Nos3</i>	0.41	0.10	0.72	6.84	2.77	1.04E-34	4.65E-32
<i>Adgrl4</i>	0.43	0.11	0.74	6.77	2.76	8.60E-36	4.01E-33
<i>Col18a1</i>	0.44	0.12	0.77	6.64	2.73	1.92E-36	9.61E-34
<i>AU021092</i>	0.39	0.10	0.67	6.55	2.71	1.87E-32	7.65E-30
<i>Slco1c1</i>	0.40	0.11	0.70	6.49	2.70	4.12E-33	1.73E-30
<i>Itm2a</i>	0.99	0.27	1.72	6.30	2.65	9.91E-77	1.41E-73
<i>Slc1a4</i>	0.59	0.16	1.01	6.17	2.62	9.36E-46	6.01E-43
<i>Zic3</i>	0.52	0.15	0.89	6.15	2.62	1.19E-40	6.66E-38
<i>Tspan18</i>	0.50	0.14	0.85	5.85	2.55	3.01E-37	1.55E-34
<i>Lmo2</i>	0.60	0.18	1.02	5.79	2.53	4.09E-44	2.44E-41
<i>Tfrc</i>	0.67	0.20	1.15	5.77	2.53	1.45E-49	1.05E-46
<i>Ramp2</i>	0.68	0.20	1.17	5.74	2.52	2.80E-50	2.07E-47
<i>Rasip1</i>	0.41	0.12	0.70	5.72	2.52	2.68E-30	9.69E-28
<i>Lsr</i>	0.38	0.11	0.64	5.69	2.51	9.28E-28	3.07E-25
<i>Slc40a1</i>	0.50	0.15	0.85	5.59	2.48	6.17E-36	2.96E-33
<i>Myo10</i>	0.69	0.21	1.18	5.56	2.48	1.92E-49	1.36E-46
<i>Eogt</i>	0.40	0.12	0.67	5.54	2.47	1.11E-28	3.86E-26
<i>Limch1</i>	0.45	0.14	0.76	5.49	2.46	1.07E-31	4.08E-29
<i>Sox18</i>	0.33	0.10	0.56	5.48	2.45	6.61E-24	1.89E-21
<i>Plxnd1</i>	0.43	0.14	0.73	5.36	2.42	1.31E-30	4.84E-28
<i>Mpzl1</i>	0.55	0.17	0.93	5.33	2.41	9.54E-38	5.07E-35
<i>Slc39a8</i>	0.40	0.13	0.67	5.26	2.40	9.99E-28	3.27E-25
<i>Adgrf5</i>	0.50	0.16	0.83	5.26	2.40	8.70E-34	3.80E-31
<i>Aplnr</i>	0.32	0.10	0.54	5.23	2.39	2.82E-22	7.26E-20
<i>Slc6a6</i>	1.05	0.35	1.76	5.08	2.34	7.13E-68	8.37E-65
<i>Slc38a2</i>	2.31	0.77	3.86	5.03	2.33	1.32E-134	4.07E-131
<i>Abcb1a</i>	0.31	0.10	0.51	4.92	2.30	4.16E-20	9.83E-18
<i>Pmp</i>	0.49	0.17	0.81	4.92	2.30	2.15E-31	8.06E-29
<i>Tsc22d1</i>	2.10	0.71	3.48	4.87	2.29	6.04E-123	1.58E-119
<i>Slc39a10</i>	0.61	0.21	1.01	4.72	2.24	6.00E-38	3.24E-35
<i>Apod</i>	0.90	0.32	1.49	4.68	2.23	2.84E-54	2.42E-51
<i>Lrp8</i>	0.38	0.14	0.62	4.55	2.18	8.99E-23	2.39E-20
<i>Thsd1</i>	0.30	0.11	0.49	4.54	2.18	4.32E-18	9.20E-16
<i>Robo4</i>	0.28	0.10	0.46	4.53	2.18	1.35E-17	2.72E-15
<i>Ccnj1</i>	0.38	0.14	0.63	4.51	2.17	3.75E-23	1.03E-20
<i>Enpp2</i>	0.29	0.10	0.47	4.50	2.17	2.17E-17	4.30E-15
<i>Apln</i>	0.29	0.10	0.47	4.48	2.16	2.17E-17	4.30E-15
<i>Pivap</i>	0.30	0.11	0.50	4.47	2.16	8.61E-19	1.91E-16
<i>Bsg</i>	0.97	0.36	1.58	4.43	2.15	1.36E-54	1.18E-51
<i>Sox17</i>	0.28	0.10	0.45	4.42	2.14	5.71E-17	1.09E-14
<i>Nampt</i>	0.49	0.18	0.81	4.40	2.14	1.89E-28	6.49E-26
<i>Palmd</i>	0.31	0.11	0.50	4.39	2.13	2.57E-18	5.56E-16
<i>Eng</i>	0.49	0.18	0.80	4.37	2.13	3.94E-28	1.31E-25
<i>Kank3</i>	0.30	0.11	0.49	4.36	2.12	4.87E-18	1.03E-15
<i>Tek</i>	0.40	0.15	0.65	4.34	2.12	1.16E-22	3.05E-20
<i>Pde8a</i>	0.33	0.12	0.53	4.33	2.12	8.93E-19	1.97E-16
<i>Ctla2a</i>	0.30	0.11	0.48	4.32	2.11	3.97E-17	7.59E-15
<i>Milt4</i>	0.57	0.22	0.93	4.27	2.10	1.39E-31	5.24E-29
<i>Podxl</i>	0.31	0.12	0.50	4.27	2.10	7.15E-18	1.48E-15
<i>Dock9</i>	0.31	0.12	0.50	4.26	2.09	7.15E-18	1.48E-15
<i>Ablim1</i>	0.58	0.22	0.94	4.24	2.08	2.88E-32	1.17E-29
<i>Gja1</i>	0.28	0.11	0.45	4.19	2.07	4.57E-16	8.14E-14
<i>Ece1</i>	0.31	0.12	0.49	4.13	2.05	7.03E-17	1.32E-14

<i>Myh10</i>	0.85	0.33	1.37	4.12	2.04	1.04E-44	6.43E-42
<i>Erg</i>	0.26	0.10	0.41	4.10	2.03	2.53E-14	4.01E-12
<i>Esam</i>	0.69	0.27	1.11	4.06	2.02	5.78E-36	2.81E-33
<i>Gm28045 Prnd</i>	0.25	0.10	0.40	4.02	2.01	1.47E-13	2.18E-11
<i>Mecom</i>	0.27	0.11	0.43	4.01	2.00	1.35E-14	2.19E-12
<i>Cyrr1</i>	0.27	0.11	0.43	4.00	2.00	2.07E-14	3.32E-12
<i>Sh3bp5</i>	0.42	0.17	0.68	4.00	2.00	6.14E-22	1.57E-19
<i>Adm</i>	0.31	0.12	0.49	3.99	2.00	2.09E-16	3.83E-14
<i>Kcp</i>	0.34	0.14	0.54	3.98	1.99	3.82E-18	8.23E-16
<i>Ccdc42ep3</i>	0.31	0.13	0.49	3.94	1.98	4.64E-16	8.22E-14
<i>Sema6a</i>	0.65	0.26	1.04	3.93	1.98	2.95E-32	1.18E-29
<i>Fil1</i>	0.40	0.16	0.64	3.89	1.96	1.58E-20	3.81E-18
<i>Ccdc141</i>	0.39	0.16	0.62	3.87	1.95	7.16E-20	1.67E-17
<i>Ptpn2</i>	0.48	0.20	0.77	3.87	1.95	2.69E-24	7.91E-22
<i>Plk2</i>	0.34	0.14	0.54	3.82	1.93	2.88E-17	5.57E-15
<i>Ecsr</i>	0.38	0.16	0.60	3.82	1.93	2.14E-19	4.93E-17
<i>Dok4</i>	0.27	0.11	0.43	3.80	1.93	4.26E-14	6.65E-12
<i>Csrp2</i>	0.47	0.20	0.74	3.76	1.91	1.11E-22	2.92E-20
<i>Lef1</i>	0.29	0.12	0.46	3.76	1.91	1.61E-14	2.58E-12
<i>Fn1</i>	1.23	0.52	1.95	3.75	1.91	4.92E-57	4.78E-54
<i>Efna1</i>	0.25	0.11	0.40	3.72	1.90	1.61E-12	2.19E-10
<i>Slc3a2</i>	1.80	0.77	2.83	3.69	1.88	1.96E-80	3.18E-77
<i>Sox7</i>	0.24	0.10	0.38	3.68	1.88	8.83E-12	1.15E-09
<i>Adamtsl2</i>	0.23	0.10	0.37	3.67	1.88	1.12E-11	1.43E-09
<i>Abca1</i>	0.93	0.40	1.46	3.67	1.88	3.11E-42	1.76E-39
<i>Tdrp</i>	0.24	0.10	0.37	3.62	1.86	6.17E-12	8.11E-10
<i>Apcdd1</i>	0.28	0.12	0.44	3.60	1.85	1.87E-13	2.67E-11

Table S6

Related to Figure 2

List of genes most strongly enriched in the microglia cluster of the scRNA-seq dataset.

Gene	Base Mean	Base MeanA	Base MeanB	fold-enrichment	log2 [enrichment]	p value	FDR
<i>C1qb</i>	3.56	0.20	6.93	34.99	5.13	0.00E+00	0.00E+00
<i>Ctss</i>	2.87	0.17	5.57	33.32	5.06	0.00E+00	0.00E+00
<i>C1qc</i>	2.13	0.14	4.13	29.80	4.90	0.00E+00	0.00E+00
<i>Csf1r</i>	2.28	0.15	4.40	28.70	4.84	0.00E+00	0.00E+00
<i>Ly86</i>	1.76	0.12	3.39	27.79	4.80	7.45E-222	2.54E-218
<i>Hexb</i>	2.26	0.18	4.34	24.59	4.62	0.00E+00	0.00E+00
<i>Ccl4</i>	1.33	0.12	2.53	21.13	4.40	1.72E-155	3.08E-152
<i>Cx3cr1</i>	1.38	0.12	2.64	21.12	4.40	4.75E-161	1.01E-157
<i>P2ry12</i>	1.25	0.11	2.38	20.79	4.38	8.41E-145	1.30E-141
<i>Fcer1g</i>	1.38	0.13	2.62	20.05	4.33	9.43E-158	1.78E-154
<i>Fcrls</i>	1.24	0.12	2.35	19.62	4.29	1.46E-141	2.16E-138
<i>Apoe</i>	7.48	0.76	14.21	18.62	4.22	0.00E+00	0.00E+00
<i>Mpeg1</i>	1.15	0.12	2.18	18.48	4.21	5.02E-129	6.84E-126
<i>C3ar1</i>	1.18	0.12	2.24	18.02	4.17	7.47E-131	1.06E-127
<i>Ctsd</i>	2.35	0.25	4.45	17.67	4.14	0.00E+00	0.00E+00
<i>Ctsb</i>	4.30	0.47	8.13	17.24	4.11	0.00E+00	0.00E+00
<i>Lgmn</i>	1.52	0.17	2.88	17.05	4.09	5.47E-165	1.24E-161
<i>C1qa</i>	0.99	0.11	1.87	16.55	4.05	1.13E-106	1.33E-103
<i>Tyrobp</i>	0.87	0.11	1.64	15.01	3.91	1.02E-90	1.06E-87
<i>Cd53</i>	0.96	0.14	1.78	12.92	3.69	6.42E-94	6.83E-91
<i>Laptm5</i>	1.96	0.30	3.63	11.96	3.58	3.23E-179	7.84E-176
<i>Kctd12</i>	0.95	0.16	1.73	11.17	3.48	6.03E-86	5.86E-83
<i>Atf3</i>	1.46	0.26	2.66	10.32	3.37	4.75E-126	6.22E-123
<i>Lyz1 Lyz2</i>	0.64	0.11	1.16	10.24	3.36	3.82E-56	2.50E-53
<i>Fcgr3</i>	0.62	0.11	1.13	10.07	3.33	2.52E-54	1.56E-51
<i>Hpgds</i>	0.67	0.12	1.22	10.06	3.33	9.10E-58	6.20E-55
<i>Gm</i>	1.92	0.35	3.48	9.99	3.32	1.08E-159	2.16E-156
<i>Plek</i>	0.61	0.11	1.10	9.71	3.28	1.21E-51	7.00E-49
<i>Ccl3</i>	0.71	0.14	1.29	9.40	3.23	2.24E-59	1.66E-56
<i>Cd83</i>	0.66	0.13	1.20	9.37	3.23	6.01E-55	3.86E-52
<i>Coro1a</i>	0.58	0.11	1.06	9.25	3.21	6.79E-48	3.67E-45
<i>Ctsl</i>	1.49	0.30	2.68	8.97	3.16	3.02E-118	3.80E-115
<i>Aif1</i>	0.54	0.11	0.97	8.91	3.15	1.28E-43	6.04E-41
<i>Siglech</i>	0.51	0.10	0.91	8.76	3.13	5.42E-41	2.22E-38
<i>Cst3</i>	2.89	0.60	5.17	8.58	3.10	7.51E-194	2.32E-190
<i>Ptgs1</i>	0.53	0.11	0.95	8.49	3.09	3.89E-42	1.70E-39
<i>Sirpa</i>	0.65	0.14	1.16	8.47	3.08	3.74E-51	2.12E-48
<i>Lpl</i>	0.64	0.14	1.14	7.90	2.98	1.65E-47	8.77E-45
<i>Cd52</i>	0.45	0.10	0.79	7.65	2.94	1.77E-33	5.90E-31
<i>Bin2</i>	0.52	0.12	0.91	7.55	2.92	1.28E-37	4.85E-35
<i>Spp1</i>	0.43	0.10	0.75	7.37	2.88	3.26E-31	1.00E-28
<i>Itgam</i>	0.46	0.11	0.80	7.27	2.86	6.08E-33	2.01E-30
<i>Olfml3</i>	0.59	0.14	1.03	7.26	2.86	6.20E-42	2.67E-39
<i>Trem2</i>	0.43	0.10	0.75	7.23	2.85	7.25E-31	2.18E-28
<i>Ly6e</i>	0.76	0.19	1.34	7.23	2.85	5.09E-54	3.04E-51
<i>Ncf1</i>	0.43	0.11	0.76	7.02	2.81	2.29E-30	6.79E-28
<i>P2ry13</i>	0.43	0.11	0.76	6.90	2.79	2.29E-30	6.79E-28
<i>Cfh</i>	0.50	0.13	0.87	6.88	2.78	2.37E-34	8.16E-32
<i>B2m</i>	2.47	0.63	4.31	6.82	2.77	4.58E-148	7.80E-145
<i>Pld4</i>	0.41	0.11	0.72	6.77	2.76	1.78E-28	5.08E-26
<i>Adgre1</i>	0.40	0.10	0.70	6.76	2.76	8.69E-28	2.37E-25
<i>Evi2a</i>	0.42	0.11	0.72	6.67	2.74	7.84E-28	2.15E-25
<i>Unc93b1</i>	0.49	0.13	0.85	6.64	2.73	1.09E-32	3.47E-30
<i>Il1a</i>	0.40	0.11	0.70	6.56	2.71	3.81E-27	1.01E-24
<i>Fyb</i>	0.40	0.11	0.70	6.55	2.71	1.21E-26	3.16E-24
<i>Psap</i>	1.14	0.31	1.97	6.45	2.69	1.40E-72	1.17E-69
<i>Apbb1ip</i>	0.38	0.10	0.65	6.42	2.68	4.36E-25	1.02E-22
<i>Cd180</i>	0.36	0.10	0.63	6.17	2.63	1.34E-23	2.92E-21
<i>Cd33</i>	0.40	0.11	0.70	6.06	2.60	1.98E-25	4.78E-23
<i>Il6ra</i>	0.40	0.12	0.69	5.99	2.58	1.98E-25	4.78E-23
<i>Cyth4</i>	0.39	0.11	0.67	5.99	2.58	1.47E-24	3.37E-22
<i>Ctsz</i>	0.85	0.25	1.45	5.93	2.57	9.97E-51	5.48E-48
<i>Tgfbr1</i>	0.73	0.21	1.25	5.88	2.56	4.12E-43	1.92E-40
<i>Pde3b</i>	0.43	0.12	0.73	5.87	2.55	6.47E-26	1.61E-23
<i>Nckap1l</i>	0.36	0.11	0.61	5.79	2.53	4.86E-22	9.62E-20
<i>Gpr34</i>	0.35	0.10	0.60	5.78	2.53	7.63E-22	1.50E-19
<i>Rnase4</i>	0.80	0.24	1.36	5.77	2.53	2.12E-46	1.08E-43
<i>Rac2</i>	0.37	0.11	0.63	5.72	2.52	3.76E-22	7.49E-20
<i>Arhgap25</i>	0.44	0.13	0.74	5.61	2.49	9.54E-26	2.34E-23
<i>Serinc3</i>	2.18	0.67	3.69	5.51	2.46	4.48E-113	5.45E-110
<i>Ctsc</i>	0.57	0.18	0.96	5.34	2.42	1.86E-31	5.75E-29
<i>Man2b1</i>	0.48	0.15	0.80	5.34	2.42	1.33E-26	3.47E-24
<i>Pou2f2</i>	0.46	0.15	0.78	5.33	2.41	5.32E-26	1.33E-23

<i>Myo1f</i>	0.33	0.11	0.56	5.29	2.40	9.81E-19	1.63E-16
<i>Tpd52</i>	0.43	0.14	0.73	5.23	2.39	5.22E-24	1.16E-21
<i>Ptpn6</i>	0.40	0.13	0.68	5.21	2.38	1.53E-22	3.18E-20
<i>Lpcat2</i>	0.32	0.10	0.54	5.20	2.38	2.84E-18	4.65E-16
<i>Ptprc</i>	0.34	0.11	0.57	5.19	2.38	3.87E-19	6.55E-17
<i>Maf</i>	0.68	0.22	1.14	5.17	2.37	7.56E-37	2.77E-34
<i>Selplg</i>	0.33	0.11	0.55	5.17	2.37	2.84E-18	4.65E-16
<i>Gusb</i>	0.66	0.22	1.10	5.07	2.34	2.30E-34	7.98E-32
<i>Ncf2</i>	0.38	0.13	0.64	5.02	2.33	1.65E-20	3.04E-18
<i>Rgs10</i>	0.39	0.13	0.65	5.00	2.32	3.64E-21	6.85E-19
<i>Mt1</i>	0.43	0.14	0.72	4.97	2.31	2.42E-22	4.87E-20
<i>Cd9</i>	0.49	0.16	0.81	4.96	2.31	2.80E-25	6.63E-23
<i>Abhd12</i>	0.46	0.16	0.77	4.86	2.28	9.00E-24	1.98E-21
<i>Lgals9</i>	0.46	0.16	0.77	4.84	2.28	9.00E-24	1.98E-21
<i>Trib1</i>	0.59	0.20	0.97	4.82	2.27	3.73E-29	1.07E-26
<i>Cd84</i>	0.32	0.11	0.53	4.76	2.25	3.47E-16	5.14E-14
<i>Arpc1b</i>	1.23	0.43	2.03	4.74	2.25	5.23E-59	3.71E-56
<i>Neat1</i>	0.42	0.15	0.70	4.73	2.24	2.04E-21	3.87E-19
<i>Plin2</i>	0.51	0.18	0.83	4.62	2.21	1.05E-24	2.42E-22
<i>Ifrd1</i>	0.69	0.25	1.14	4.62	2.21	8.82E-33	2.89E-30
<i>Vsir</i>	0.36	0.13	0.59	4.59	2.20	7.76E-18	1.25E-15
<i>Runx1</i>	0.32	0.11	0.52	4.57	2.19	1.00E-15	1.44E-13
<i>Parvg</i>	0.30	0.11	0.49	4.55	2.19	6.75E-15	9.26E-13
<i>Ifi30</i>	0.36	0.13	0.59	4.55	2.18	1.31E-17	2.09E-15
<i>Hexa</i>	0.46	0.17	0.75	4.52	2.18	1.57E-21	3.02E-19
<i>Sgpl1</i>	0.44	0.16	0.71	4.51	2.17	1.05E-20	1.94E-18
<i>Arl4c</i>	0.40	0.15	0.66	4.49	2.17	4.89E-19	8.21E-17

Table S7

Related to Figure 3

Top 50 enriched genes in the EMBRACE-isolated neural population (CD45^{neg}, CD41^{neg}, CD11b^{neg}, PECAM1^{neg}, CD102^{neg}, PDGFR β ^{neg}).

Gene	baseMean	log2FC	p value	FDR
<i>Gm42418</i>	4045.63	15.89	3.35E-88	6.93E-85
<i>Ptpn2</i>	294.82	11.60	6.49E-55	3.42E-52
<i>Slc32a1</i>	220.18	11.50	3.14E-55	1.72E-52
<i>Gm8203</i>	177.07	11.48	1.41E-49	5.10E-47
<i>Xkr7</i>	169.99	11.43	2.44E-50	9.79E-48
<i>Ecel1</i>	166.55	11.40	3.71E-49	1.31E-46
<i>Pdcd2</i>	132.45	11.08	1.11E-46	3.44E-44
<i>Myo16</i>	194.24	11.02	5.57E-53	2.63E-50
<i>Nalcn</i>	119.54	10.93	1.08E-45	3.19E-43
<i>Shisa6</i>	106.85	10.77	1.68E-43	4.30E-41
<i>Gpr26</i>	129.34	10.74	4.48E-47	1.43E-44
<i>Uncx</i>	157.31	10.69	1.16E-43	3.02E-41
<i>Gjd2</i>	90.05	10.52	4.59E-41	9.78E-39
<i>Tmem28</i>	106.58	10.46	7.67E-43	1.89E-40
<i>Fam189a1</i>	105.19	10.45	1.83E-44	4.97E-42
<i>Rtn4r</i>	85.74	10.44	6.58E-38	1.14E-35
<i>Reln</i>	1791.73	10.40	6.61E-18	2.21E-16
<i>Grm4</i>	79.77	10.35	1.27E-39	2.42E-37
<i>Islr2</i>	4212.44	10.33	2.29E-31	2.54E-29
<i>Lrrn2</i>	270.23	10.25	3.59E-65	3.32E-62
<i>Tmem59l</i>	111.39	10.23	3.44E-45	9.72E-43
<i>Kndc1</i>	90.12	10.23	1.93E-42	4.52E-40
<i>Erbb4</i>	334.30	10.20	2.55E-63	2.21E-60
<i>Gm12481</i>	69.70	10.14	3.11E-35	4.52E-33
<i>Miat</i>	13098.89	10.09	2.87E-46	8.66E-44
<i>Gm5812</i>	64.73	10.05	8.99E-37	1.50E-34
<i>Hrh3</i>	76.46	10.00	4.83E-39	8.89E-37
<i>Gabra3</i>	141.92	10.00	5.50E-47	1.74E-44
<i>Mmp24</i>	430.49	9.99	1.46E-11	2.30E-10
<i>Galnt14</i>	61.39	9.98	5.85E-36	9.08E-34
<i>Zim1</i>	94.94	9.96	2.45E-35	3.60E-33
<i>Sorcs3</i>	75.21	9.95	3.73E-36	5.96E-34
<i>Magel2</i>	868.39	9.94	2.44E-27	2.01E-25
<i>Frmpd3</i>	91.12	9.92	1.82E-37	3.10E-35
<i>Epha8</i>	87.93	9.90	2.04E-41	4.42E-39
<i>Chrna3</i>	56.23	9.84	1.61E-33	2.18E-31
<i>Kcnf1</i>	66.83	9.80	1.81E-38	3.25E-36
<i>Disp2</i>	604.76	9.78	9.20E-14	1.93E-12
<i>Thsd7b</i>	65.77	9.76	4.70E-36	7.38E-34
<i>Gm996</i>	63.80	9.74	2.76E-38	4.85E-36
<i>Gm27032</i>	51.06	9.71	8.27E-34	1.13E-31
<i>Scg2</i>	118.04	9.69	5.71E-18	1.92E-16
<i>Tunar</i>	47.92	9.62	3.46E-32	4.22E-30
<i>Tenm1</i>	73.28	9.57	1.08E-30	1.12E-28
<i>Zfhx2os</i>	56.80	9.57	2.86E-36	4.63E-34
<i>Lgi2</i>	46.12	9.57	3.54E-32	4.31E-30
<i>Rgs7</i>	46.23	9.56	2.44E-30	2.46E-28
<i>Adcyap1</i>	44.62	9.51	2.42E-31	2.68E-29
<i>Syde2</i>	54.11	9.50	7.23E-36	1.12E-33
<i>Cnpy1</i>	357.67	9.38	2.14E-16	6.08E-15

Table S8

Related to Figure 3

Top 50 enriched genes in the EMBRACE-isolated mural cell population ($\text{PDGFR}\beta^{\text{high}}$, $\text{PECAM1}^{\text{neg}}$, $\text{CD102}^{\text{neg}}$, CD45^{neg} , CD41^{neg} , $\text{CD11b}^{\text{neg}}$). Due to their high abundance in the list, genes with the Gm prefix were removed from this list.

Gene	baseMean	log2FC	p value	FDR
<i>Kcne4</i>	933.90	12.51	1.60E-38	4.74E-35
<i>Cpa1</i>	309.65	11.90	9.97E-44	4.72E-40
<i>Ednra</i>	5589.26	11.86	2.58E-43	1.02E-39
<i>Atp13a5</i>	616.11	10.83	3.05E-18	1.90E-15
<i>Enpep</i>	222.42	10.58	1.57E-47	9.30E-44
<i>Mmp9</i>	11155.83	10.36	6.24E-20	5.09E-17
<i>Alx1</i>	156.94	10.25	2.15E-29	3.91E-26
<i>Hcar1</i>	87.23	10.23	1.15E-21	1.23E-18
<i>Slc6a20a</i>	254.82	10.03	2.22E-18	1.46E-15
<i>4933431K23Rik</i>	69.23	9.75	3.23E-26	4.78E-23
<i>Rarres2</i>	185.96	9.74	2.22E-35	5.83E-32
<i>Vtn</i>	12818.27	9.42	3.07E-15	1.17E-12
<i>B830012L14Rik</i>	214.23	9.27	1.53E-59	1.81E-55
<i>Sod3</i>	359.20	9.26	4.10E-31	8.82E-28
<i>8030451A03Rik</i>	84.20	9.05	3.30E-16	1.62E-13
<i>Tbx18</i>	406.60	8.69	2.12E-15	8.51E-13
<i>Akr1c12</i>	33.37	8.68	1.15E-11	2.12E-09
<i>Vpreb3</i>	30.63	8.61	4.61E-20	3.90E-17
<i>Cd248</i>	1895.31	8.12	2.09E-17	1.12E-14
<i>Art3</i>	1845.52	8.07	6.34E-24	7.89E-21
<i>Ins2</i>	22.41	8.03	5.27E-09	4.95E-07
<i>Slc38a11</i>	137.30	7.98	2.29E-19	1.75E-16
<i>Postn</i>	605.46	7.86	1.90E-15	7.76E-13
<i>C1qtnf2</i>	86.03	7.84	9.73E-16	4.19E-13
<i>Myocd</i>	30.12	7.81	6.25E-15	2.24E-12
<i>1600015I10Rik</i>	15.33	7.71	2.61E-10	3.52E-08
<i>4921534H16Rik</i>	16.11	7.61	2.30E-08	1.84E-06
<i>Mylk4</i>	86.57	7.57	2.05E-22	2.31E-19
<i>Vstm4</i>	663.01	7.55	4.08E-07	2.27E-05
<i>Ndufa4l2</i>	6822.54	7.55	2.89E-10	3.83E-08
<i>Cspg4</i>	2288.33	7.50	5.72E-12	1.14E-09
<i>Krtdap</i>	16.93	7.44	1.73E-06	7.67E-05
<i>Kcnmb1</i>	228.04	7.43	2.18E-08	1.75E-06
<i>Myl9</i>	8993.35	7.31	2.34E-24	3.08E-21
<i>S1pr3</i>	3632.06	7.28	5.15E-06	1.91E-04
<i>S1pr3</i>	3632.06	7.28	5.15E-06	0.000191
<i>Npn2</i>	12.38	7.25	1.29E-07	8.36E-06
<i>2010003K11Rik</i>	14.42	7.25	0.000873	0.010468
<i>Col6a3</i>	192.08	7.23	4.75E-07	2.56E-05
<i>Rgs4</i>	13901.09	7.21	9.88E-09	8.63E-07
<i>Prss45</i>	11.53	7.20	6.59E-08	4.64E-06
<i>Bmp5</i>	317.08	7.20	5.23E-07	2.78E-05
<i>Lamc3</i>	717.82	7.15	1.01E-07	6.79E-06
<i>C1qtnf7</i>	13.84	7.14	5.78E-09	5.34E-07
<i>Gpr20</i>	56.94	7.14	2.08E-08	1.69E-06
<i>Tmc5</i>	112.89	7.14	2.50E-07	1.50E-05
<i>Des</i>	125.96	7.12	2.75E-08	2.16E-06
<i>Tnxb</i>	106.90	7.11	6.84E-08	4.79E-06
<i>Crygc</i>	10.94	7.06	4.19E-07	2.32E-05
<i>Higd1b</i>	2370.20	7.00	8.42E-04	1.02E-02

Table S9

Related to Figure 3

Top 50 enriched genes in the EMBRACE-isolated endothelial cell population (PECAM1^{pos}, CD102^{pos}, CD45^{neg}, CD41^{neg}, CD11b^{neg}, PDGFR β ^{neg}).

Gene	baseMean	log2FC	p value	FDR
<i>Myct1</i>	675.89	12.81	1.24E-57	1.43E-53
<i>Mogat2</i>	510.34	12.66	4.39E-44	2.53E-40
<i>Gimap4</i>	332.25	12.38	8.88E-31	1.86E-27
<i>Kcnex3</i>	362.22	12.19	3.43E-21	3.44E-18
<i>Tbx1</i>	339.36	11.70	4.42E-30	8.48E-27
<i>Gm38197</i>	377.99	11.45	1.09E-31	3.15E-28
<i>Mall</i>	212.27	11.43	4.55E-26	6.97E-23
<i>Igfs5</i>	101.69	10.67	2.16E-20	1.85E-17
<i>Cfi</i>	107.66	10.44	1.54E-33	5.05E-30
<i>Nos3</i>	1955.22	10.35	7.87E-34	3.02E-30
<i>4930578C19Rik</i>	85.41	9.91	8.92E-11	1.35E-08
<i>A530016L24Rik</i>	62.83	9.75	1.01E-12	2.38E-10
<i>Gm37393</i>	60.31	9.73	3.53E-13	9.23E-11
<i>Gm694</i>	47.25	9.73	7.35E-20	5.83E-17
<i>Cldn5</i>	14488.32	9.54	3.02E-09	3.26E-07
<i>Rassf9</i>	951.34	9.30	4.94E-13	1.23E-10
<i>Gm12866</i>	37.97	9.29	8.43E-15	2.85E-12
<i>Rp1</i>	108.20	9.28	1.92E-24	2.60E-21
<i>Foxl2</i>	237.78	9.27	1.61E-24	2.32E-21
<i>Ces2b</i>	53.19	9.22	4.80E-09	4.80E-07
<i>BB365896</i>	39.02	9.12	4.63E-17	2.42E-14
<i>Cica2</i>	51.76	9.02	1.13E-10	1.67E-08
<i>Slc38a5</i>	6137.35	9.00	4.45E-12	9.40E-10
<i>Serpinb9b</i>	78.97	8.98	2.89E-14	8.98E-12
<i>9930038B18Rik</i>	30.18	8.92	9.08E-13	2.18E-10
<i>Mmrn1</i>	1127.35	8.85	6.41E-15	2.23E-12
<i>Gm38066</i>	35.10	8.85	1.36E-09	1.62E-07
<i>Psg17</i>	39.10	8.83	1.70E-15	6.54E-13
<i>Aplnr</i>	4161.45	8.75	6.14E-08	4.53E-06
<i>Gpihbp1</i>	25.07	8.72	3.72E-13	9.51E-11
<i>Unc45b</i>	275.01	8.69	5.60E-11	8.99E-09
<i>Vwa1</i>	4369.62	8.68	3.22E-16	1.51E-13
<i>Adgrl4</i>	3021.45	8.58	3.63E-12	7.80E-10
<i>Gpr143</i>	32.49	8.44	8.44E-05	2.00E-03
<i>Rhbd12</i>	262.17	8.40	1.98E-09	2.22E-07
<i>Gm24283</i>	36.06	8.40	1.53E-15	5.96E-13
<i>Hapl1</i>	232.78	8.30	8.39E-12	1.69E-09
<i>Acsgbg2</i>	20.54	8.23	4.01E-09	4.18E-07
<i>Myzap</i>	406.72	8.20	2.11E-11	3.73E-09
<i>Slco1c1</i>	1776.55	8.20	4.04E-11	6.69E-09
<i>Allc</i>	22.61	8.15	3.07E-10	4.22E-08
<i>Ushbp1</i>	1659.27	8.13	9.69E-14	2.79E-11
<i>Ptgis</i>	730.64	8.03	9.58E-10	1.18E-07
<i>Shbg</i>	32.10	8.01	1.37E-09	1.63E-07
<i>T</i>	121.42	7.97	2.40E-10	3.37E-08
<i>Prnd</i>	159.22	7.92	3.75E-12	8.00E-10
<i>Tecrl</i>	18.10	7.86	2.62E-04	4.75E-03
<i>Gm10258</i>	22.95	7.84	8.03E-06	2.95E-04
<i>Nos2</i>	173.31	7.84	3.26E-10	4.47E-08
<i>Foxl2os</i>	56.12	7.84	2.04E-13	5.65E-11

Table S10

Related to Figure 3

Top 50 enriched genes in the EMBRACE-isolated microglia population (CD45^{medium}, CD11b^{pos}, PECAM1^{neg}, PDGFR β ^{neg}).

Gene	baseMean	log2FC	p value	FDR
<i>Ctss</i>	17584.46	17.68	2.32E-101	1.34E-97
<i>Fcrls</i>	15462.25	17.49	2.86E-99	1.32E-95
<i>C1qc</i>	13028.88	17.28	1.30E-101	9.95E-98
<i>C1qb</i>	17918.06	17.00	9.11E-130	1.05E-125
<i>Fcgr3</i>	7037.22	16.41	8.74E-90	3.36E-86
<i>Ly86</i>	4920.81	15.86	1.77E-77	3.72E-74
<i>Trem2</i>	4014.58	15.60	3.87E-78	8.92E-75
<i>Adgre1</i>	4387.59	15.24	3.40E-89	1.12E-85
<i>C1qa</i>	6834.11	15.16	1.14E-65	1.46E-62
<i>Cd86</i>	2583.89	15.14	1.60E-53	1.19E-50
<i>Rgs1</i>	1985.73	14.89	2.03E-61	2.34E-58
<i>Cd84</i>	2662.58	14.87	1.88E-55	1.61E-52
<i>Siglech</i>	3729.47	14.83	7.10E-76	1.28E-72
<i>Tyrobp</i>	4861.84	14.64	2.33E-41	1.12E-38
<i>Rac2</i>	3191.76	14.64	1.21E-73	1.86E-70
<i>Spi1</i>	3588.60	14.36	1.16E-78	2.98E-75
<i>Clec5a</i>	891.88	13.80	2.07E-54	1.64E-51
<i>Ms4a6d</i>	926.47	13.73	3.11E-44	1.59E-41
<i>Ncf4</i>	831.95	13.69	8.01E-53	5.77E-50
<i>Tifab</i>	957.65	13.57	7.27E-57	7.28E-54
<i>Ms4a6b</i>	924.84	13.51	2.27E-54	1.75E-51
<i>Ms4a6c</i>	760.16	13.51	2.13E-46	1.17E-43
<i>Cd53</i>	3796.61	13.49	5.30E-55	4.36E-52
<i>Abcg3</i>	828.87	13.35	1.77E-52	1.20E-49
<i>Sash3</i>	1171.07	13.34	2.82E-59	2.95E-56
<i>Cd300c2</i>	769.03	13.31	1.25E-59	1.37E-56
<i>Ccr1</i>	612.11	13.06	3.84E-35	1.38E-32
<i>Bank1</i>	644.68	13.05	1.27E-55	1.17E-52
<i>Cx3cr1</i>	13140.39	13.04	1.92E-39	8.06E-37
<i>Tnfaip8l2</i>	629.37	12.96	2.04E-49	1.24E-46
<i>Ccl12</i>	527.37	12.94	1.37E-38	5.53E-36
<i>Clec7a</i>	525.75	12.91	5.20E-37	2.00E-34
<i>Itgam</i>	1330.38	12.88	4.69E-66	6.36E-63
<i>Nlrp3</i>	826.51	12.85	1.76E-55	1.56E-52
<i>Cd48</i>	466.81	12.84	7.48E-43	3.67E-40
<i>Casp1</i>	706.43	12.82	1.63E-52	1.14E-49
<i>Dock2</i>	2034.59	12.81	3.76E-29	9.11E-27
<i>Ptprc</i>	4962.73	12.81	2.46E-37	9.62E-35
<i>Ly9</i>	405.13	12.70	4.00E-46	2.10E-43
<i>Ccl9</i>	656.87	12.66	6.82E-48	3.93E-45
<i>A130071D04Rik</i>	596.88	12.65	8.07E-33	2.55E-30
<i>I11b</i>	396.85	12.60	1.40E-40	6.21E-38
<i>Gm1966</i>	423.74	12.60	1.50E-34	5.24E-32
<i>Cd300lf</i>	394.87	12.52	3.72E-35	1.36E-32
<i>Blnk</i>	1015.81	12.35	1.42E-70	2.05E-67
<i>Nlrp1b</i>	388.92	12.31	1.83E-46	1.03E-43
<i>Crybb1</i>	2631.46	12.20	2.47E-19	2.79E-17
<i>Aif1</i>	5410.21	12.20	2.00E-22	2.93E-20
<i>Fcgr2b</i>	339.37	12.16	2.28E-48	1.34E-45
<i>Bcl2a1b</i>	268.20	12.11	4.77E-41	2.20E-38

TRANSPARENT METHODS

Animals

All animal studies were performed according to the German animal care and ethics legislation and approved by the Committee on Research Animal Care, Regierungspräsidium Freiburg. Mice were maintained on a C57BL/6 background, under a 12-hour light and dark cycle and water and standard chow were provided ad libitum. The morning after a vaginal plug was detected was designated E0.5.

Brain dissociation

Brains from E14.5 embryos were acutely isolated and meninges were removed under a dissecting microscope. Four methods were trialed, with Liberase + DNase I performing the best according to cell survival, overall digestion as well as the retention of cell surface markers (Table S1). Each of the methodologies is detailed below.

Liberase and DNase I

E14.5 brains were transferred to 1.5 ml eppendorf tubes. To each tube, 475 µl of PBS containing 5 mM MgCl₂, 20 µl DNase I (final concentration 80 U/ml, New England Biolabs #M0303) and 5 µl Liberase TM (final concentration 0.13 WU/ml, Roche 05401119001) were added. Samples were incubated in a thermomixer (37°C, 800 rpm) for 40 minutes. Samples were gently triturated using a P1000 pipette at 20 minutes and again at the end of the 40 minutes. Samples were filtered through a 100 µm sieve and cells collected by centrifugation (250 g, room temperature, 4 minutes, swing bucket rotor) and resuspended in FACS buffer (PBS supplemented with 2% fetal calf serum).

The same methodology was used for the *Liberase only* test, with the exception that DNase I was excluded.

Pancreatin trypsin

Embryonic E14.5 brains were transferred to 500 µl dissociation solution containing 2.5% w/v pancreatin (Sigma P3292) and 0.5% w/v trypsin (Gibco 27250-018) in PBS. Tubes were incubated on ice for 30 minutes and flicked occasionally to ensure mixing. After 30 minutes, the dissociation solution was removed and samples incubated at 37°C for 5 minutes in a water bath. Next, 2% FCS / PBS was added and the brains mechanically dissociated using a P1000 pipette and passed through a 100 µm sieve prior to analysis.

Collagenase and dispase

Collagenase and Dispase were purchased from Roche (10269638001) and used according to the manufacturer's recommendations at a concentration of 1 mg/ml (w/v).

No enzyme

E14.5 brains were placed in FACS buffer and triturated ~10 times using a P1000 pipette. Samples were collected by centrifugation (250 g, room temperature, 4 minutes, swing bucket rotor) and tested for cell viability.

Flow cytometry

Dissociated E14.5 brains were washed once in PBS supplemented with 5 mM MgCl₂. Cells were passed through a 100 µm sieve, resuspended in 400 µl FACS buffer (PBS + 2% fetal calf serum) containing the PDGFRβ antibody (R+D, Table S2) and incubated on ice for 30 minutes. After two washes in FACS buffer at 4°C, cells were resuspended in 400 µl FACS buffer containing antibodies raised against CD11b, CD41, CD45, CD102 (ICAM2) and PECAM1 (CD31) as well as the Alexa488-conjugated anti-goat IgG (ThermoFisher A11055) at the indicated concentrations (Table S2). Zombie dye (Biolegend 423106, 1:200) was added to the mix as a viability marker. Cells were incubated on ice for 45 minutes, washed three times in ice cold FACS buffer, collected by centrifugation (250 g, 4°C) in a swinging bucket rotor and sorted on the FACS ARIA (BD Biosciences) using a 100 µm nozzle. For scRNA-seq analysis, cells were sorted into 384 well plates and processed according to the mCEL-Seq2 protocol (see below). For bulk populations, cells were collected in ice-cold FACS buffer, centrifuged (300 g, 4 minutes, 4°C) in a swing bucket rotor. Cell pellets were snap frozen and stored at -80°C. RNA from neural cells was isolated using the Qiagen mini kit (#74104), while RNA from mural cells, endothelial cells and microglia was extracted using the Qiagen miRNeasy Micro kit (#1071023). Libraries for RNA-seq of the neural population were prepared using the Illumina TruSeq library preparation kit. For mural cells, endothelial cells and microglia, cDNA was prepared from isolated RNA using the SMART-Seq v4 Ultra Low Input RNA Kit for Sequencing (Clontech 634891). Libraries were prepared using the Nextera XT DNA library preparation kit (Illumina FC-131-1096) and sequenced on the HiSeq 2500 instrument.

Single cell RNA sequencing

scRNA-seq was performed according to the mCEL-Seq2 protocol (Hashimshony et al., 2016; Herman et al., 2018). Single cells were index sorted into 384-well plates containing 240 nl of primer mix and 1.2 µl of mineral oil (Sigma-Aldrich). A FACS-ID for each individual well was assigned according to the gating strategy. The plates were centrifuged at 2200 g for 10 minutes at 4°C, snap-frozen in liquid nitrogen and stored at -80°C until processing. RNA was reverse transcribed using 160 nl of reverse transcription reaction mix and 2.2 µl of second strand reaction mix. cDNA from 96 cells was pooled together before clean up and *in vitro* transcription, generating 4 libraries from each 384-well plate. 0.8 µl of AMPure/RNAClean XP beads (Beckman Coulter) per 1 µl of sample were used during all the purification steps including the library clean up. Other steps were performed as described in the protocol (Herman et al., 2018). Libraries were sequenced on an Illumina HiSeq 3000 sequencing system (pair-end multiplexing run, high output mode) at a depth of ~200,000 reads per cell.

Bioinformatic analyses

Raw sequencing data for both single cell and bulk experiments were controlled for quality, trimmed and mapped to the reference mm10 genome using STAR (Dobin et al., 2013). The identity of reads

was identified through FeatureCount (Liao et al., 2014). For scRNA-seq analyses, the RNA expression matrices from each cell were merged and further analysed with the RaceID3 software package (Herman et al., 2018). Cells with less than 1500 unique transcripts were discarded, which left 625 cells for downstream analysis. For downstream analyses, ribosomal genes as well as the highly expressed ncRNA *Malat1* were removed. Cells were clustered using k-medoids and the clustering result was confirmed using the random forest algorithm within the RaceID3 package. Clusters from the scRNA-seq data were visualized through the two-dimension t-distributed stochastic neighbour embedding (tSNE) algorithm within the RaceID3 package. For both scRNA-seq and the bulk RNA-seq analyses, differentially expressed genes between the cell types or cell clusters were identified using DESeq2 (Love et al., 2014).

Inter-cellular ligand-receptor interaction networks were calculated based on the publically available database collated by Ramilowski and co-workers (Ramilowski et al., 2015). Mouse orthologs of human genes were obtained using the biomaRt R package (Durinck et al., 2005; Durinck et al., 2009). The connection between cell type and itself (autocrine) or another cell type (paracrine) was established if the receptor and its associated ligand were expressed in at least one of the four cell types. The ligand or receptor was considered expressed in each scRNA-seq cluster if the mean expression per cluster was higher than 0.7 normalised transcripts. In contrast, the ligand or receptor was considered expressed in the bulk RNA-seq dataset if the mean expression per cell type was higher than 10 FPKM, and the respective ligand or receptor expression in the given cell type was higher than 10% of maximal expression of the given ligand/receptor in any cell type. Directionality of a given interaction was determined by the cell type expressing the ligand. Colours in Figures 4B and S3B correspond to the cell type or cluster expressing the ligand, while the thickness of the lines is proportional to the number of interaction pairs between cell types. For visualization of interaction networks, the igraph (Csardi and Nepusz, 2006) and iTALK (Wang et al., 2019) R packages were utilized. The network of top 50 enriched interactions was generated with the additional criterion for the ligands to be enriched with an enrichment score > 0.5 in a cell type. For ranking the ligand-receptor interactions, the absolute expression (FPKM) of both the ligand and receptor in each interacting pair was taken into account. The enrichment score was calculated for each gene based on the normalized DESeq2 gene expression matrix; Mean expression of a gene across all cell types was subtracted from the expression levels of that gene in a particular cell type, and subsequently divided by the standard deviation. Thus, the enrichment score for a particular gene in a cell type represents the number of standard deviations from its mean expression across all analysed cell types.

Generation of the Brain Interactome Explorer website

The R code for generating circos plots from normalized expression values was wrapped in a shiny app using CRAN R package shiny version 1.3.2 (Chang et al., 2019) and R version 3.6. The resulting shiny app 'Brain Interactome Explorer' version 1.0.0 is served on shinyapps.io under <https://mpie.shinyapps.io/braininteractomeexplorer/>. The R code underlying the app is available under <https://github.com/maxplanck-ie/BrainInteractomeExplorer>.

Immunofluorescence

Testing of vascular PECAM1, ICAM2, PDGFR β and NG2 antibodies

Brains were isolated from E14.5 embryos, meninges removed and both cortices isolated. The dissected cortices were fixed in 4% paraformaldehyde at room temperature for 30 minutes. After brief washing, samples were stored in 100% methanol at 4°C. For staining, the cortices were washed in 50% methanol for 10 minutes, once in PBS for 10 minutes and twice in wash buffer (0.1% Triton X-100 in PBS) for 15 minutes each. Samples were blocked in 10% fetal calf serum (FCS) for 1 hour at room temperature and then incubated with primary antibodies raised against PDGFR β and PECAM1 (CD31, 1:50), diluted in wash buffer supplemented with 10% FCS, overnight at 4°C. The cortices were subsequently processed through the wash buffer three times (10 minutes each) at 4°C and then three times at room temperature. The cortices were incubated with secondary antibodies (Donkey anti-goat Alexa488, A21206, 1:400; donkey anti-rabbit Alexa555, A31572, 1:400) diluted in FACS buffer and incubated at room temperature for 2 hours. The samples were then washed three times at 4°C for 10 minutes each and subsequently three times for 1 hour at room temperature. The cortices were subsequently stained with DAPI (1:1000 diluted in PBS) for 30 minutes at room temperature and washed three times for 10 minutes each. The stained cortices were flattened, mounted in Fluoromount and imaged using the LSM780 microscope from Zeiss using the 63x oil objective. Data were processed using the Zen Blue software (Zeiss).

Immunofluorescence analyses of overlap in protein localisation

Freshly dissected E14.5 brains were fixed in 4% paraformaldehyde at room temperature for 2 hours, washed with PBS and embedded in a 25% albumin; 6% gelatine solution. Embedded samples were fixed further in 4% paraformaldehyde overnight, washed and subsequently stored in PBS until sectioning. Approximately 100 μ m thick sections were cut on a vibratome and slices were released in PBS. Each section was transferred to a well of a 24-well plate for subsequent staining. For stainings with antibodies against IBA1, APOE, LDLR, LRP1 and β III-tubulin, sections were permeabilized and blocked in PBS containing 0.5% TritonX-100 and 0.25% gelatine overnight at 4°C and all antibody incubations were carried out in PBS supplemented with 0.25% gelatine. For stainings with antibodies raised against VTN, KDR, PECAM1, LAMA4 and ITGB1, sections were permeabilised and blocked in PBS containing 0.5% Triton X-100 and 10% FCS overnight at 4°C. All samples were incubated with the respective combinations of primary antibodies (1:200) overnight at 4°C, washed four times for 30 minutes each at room temperature, and incubated with the appropriate secondary antibodies (donkey anti-goat 594 (1:250, Life Technologies #A11058), donkey anti-rabbit 488 (1:250, Life Technologies #A11055), goat anti-mouse 594 (1:250, Life Technologies #A11032), donkey anti-rabbit 555 (1:250, Life Technologies #A31572), goat anti-mouse 488 (1:250, Life Technologies #A11001)) overnight at 4°C. After a further 4 washes in PBS, samples were stained with DAPI (1:250, 20 minutes, RT), mounted onto slides with Fluoromount and imaged using the Zeiss Airyscan LSM 880 microscope with the 25x oil objective. Data were processed using the Zen Blue software (Zeiss).

Co-immunoprecipitation assays

Cell lysates were prepared in HMG150 buffer (25 mM HEPES pH 7.6, 12.5 mM MgCl₂, 10% glycerol, 150 mM KCl, 0.5% Tween-20 and Protease Inhibitor Complete Mini (Roche #04693159001)) from wild type snap frozen E14.5 brains and 250 µg of protein were used for each IP. A mixture of Protein A/G beads (Sepharose 4 Fast Flow Protein G (GE Healthcare #17-0618-05) and Protein A (GE Healthcare #17-5280-02)) were blocked by incubating with 0.2 mg/ml BSA in HMG150 for 30 minutes at 4°C. After pre-clearing brain lysates with 100 µl of a Protein A/G beads-slurry, 5 µg of the anti-APOE antibody were added and samples incubated overnight at 4°C. IPs with rabbit IgG (Rb-IgG, Abcam #ab172730) were used as controls. Next, 100 µl of blocked Protein A/G beads-slurry were added, samples incubated at 4°C for 1 hour and washed 3 times in HMG150 for 10 minutes each. Immunoprecipitated protein was eluted in ROTI-load (Roth #K929.1), boiled briefly and run on a 4-12% gradient gel (NuPAGE, Life Technologies #NP0321Box). Following transfer onto 0.45 µm PVDF membranes (ImmobilonP Membrane, Millipore #IPVH00010), membranes were blocked in 5% skim milk, incubated overnight at 4°C with antibodies raised against APOE and LRP1 (1:1000). After washing, the membranes were incubated with the HRP-conjugated anti-rabbit or anti-goat antibodies (ECL anti-rabbit HRP, GE Healthcare #NA934 and ECL anti-goat HRP, Santa Cruz #sc2354) for 1 hour at room temperature, washed and developed on the Chemi Doc System (Biorad), using the Lumi-Light reagent (Lumi Light Plus Western Blotting Substrate, Roche #12015196001).

Data and software availability

The Brain Interactome Explorer is available at <https://mpi-ie.shinyapps.io/braininteractomeexplorer/>.

Raw sequencing data have been uploaded to GEO and are available under GSE133079.

SUPPLEMENTARY REFERENCES

- Chang, W., Cheng, J., Allaire, J.J., Xie, Y., and McPherson, J. (2019). shiny: Web Application Framework for R. R package version 1.3.2. (<https://CRAN.R-project.org/package=shiny>).
- Csardi, G., and Nepusz, T. (2006). The igraph software package for complex network research. *InterJournal, Complex Systems* 1695.
- Dobin, A., Davis, C.A., Schlesinger, F., Drenkow, J., Zaleski, C., Jha, S., Batut, P., Chaisson, M., and Gingeras, T.R. (2013). STAR: ultrafast universal RNA-seq aligner. *Bioinformatics* 29, 15-21.
- Durinck, S., Moreau, Y., Kasprzyk, A., Davis, S., De Moor, B., Brazma, A., and Huber, W. (2005). BioMart and Bioconductor: a powerful link between biological databases and microarray data analysis. *Bioinformatics* 21, 3439-3440.
- Durinck, S., Spellman, P.T., Birney, E., and Huber, W. (2009). Mapping identifiers for the integration of genomic datasets with the R/Bioconductor package biomaRt. *Nat Protoc* 4, 1184-1191.
- Hashimshony, T., Senderovich, N., Avital, G., Klochendler, A., de Leeuw, Y., Anavy, L., Gennert, D., Li, S., Livak, K.J., Rozenblatt-Rosen, O., et al. (2016). CEL-Seq2: sensitive highly-multiplexed single-cell RNA-Seq. *Genome Biol* 17, 77.
- Herman, J.S., Sagar, and Grun, D. (2018). FateID infers cell fate bias in multipotent progenitors from single-cell RNA-seq data. *Nat Methods* 15, 379-386.
- Liao, Y., Smyth, G.K., and Shi, W. (2014). featureCounts: an efficient general purpose program for assigning sequence reads to genomic features. *Bioinformatics* 30, 923-930.
- Love, M.I., Huber, W., and Anders, S. (2014). Moderated estimation of fold change and dispersion for RNA-seq data with DESeq2. *Genome Biol* 15, 550.
- Ramilowski, J.A., Goldberg, T., Harshbarger, J., Kloppmann, E., Lizio, M., Satagopam, V.P., Itoh, M., Kawaji, H., Carninci, P., Rost, B., et al. (2015). A draft network of ligand-receptor-mediated multicellular signalling in human. *Nature communications* 6, 7866.
- Rosenberg, A.B., Roco, C.M., Muscat, R.A., Kuchina, A., Sample, P., Yao, Z., Graybuck, L.T., Peeler, D.J., Mukherjee, S., Chen, W., et al. (2018). Single-cell profiling of the developing mouse brain and spinal cord with split-pool barcoding. *Science* 360, 176-182.
- Sheikh, B.N., Dixon, M.P., Thomas, T., and Voss, A.K. (2012). Querkopf is a key marker of self-renewal and multipotency of adult neural stem cells. *Journal of cell science* 125, 295-309.
- Vanlandewijck, M., He, L., Mae, M.A., Andrae, J., Ando, K., Del Gaudio, F., Nahar, K., Lebouvier, T., Lavina, B., Gouveia, L., et al. (2018). A molecular atlas of cell types and zonation in the brain vasculature. *Nature* 554, 475-480.
- Wang, Y., Wang, R., Zhang, S., Song, S., Jiang, C., Han, G., Wang, M., Ajani, J., Futreal, A., and Wang, L. (2019). iTALK: an R Package to Characterize and Illustrate Intercellular Communication. *bioRxiv*.
- Zeisel, A., Hochgerner, H., Lonnerberg, P., Johnsson, A., Memic, F., van der Zwan, J., Haring, M., Braun, E., Borm, L.E., La Manno, G., et al. (2018). Molecular Architecture of the Mouse Nervous System. *Cell* 174, 999-1014 e1022.